Chemical Science



PERSPECTIVE

View Article Online
View Journal | View Issue



Cite this: Chem. Sci., 2021, 12, 3406

All publication charges for this article have been paid for by the Royal Society of Chemistry

Received 19th December 2020 Accepted 16th January 2021

DOI: 10.1039/d0sc06928k

rsc.li/chemical-science

Fluorescent small organic probes for biosensing

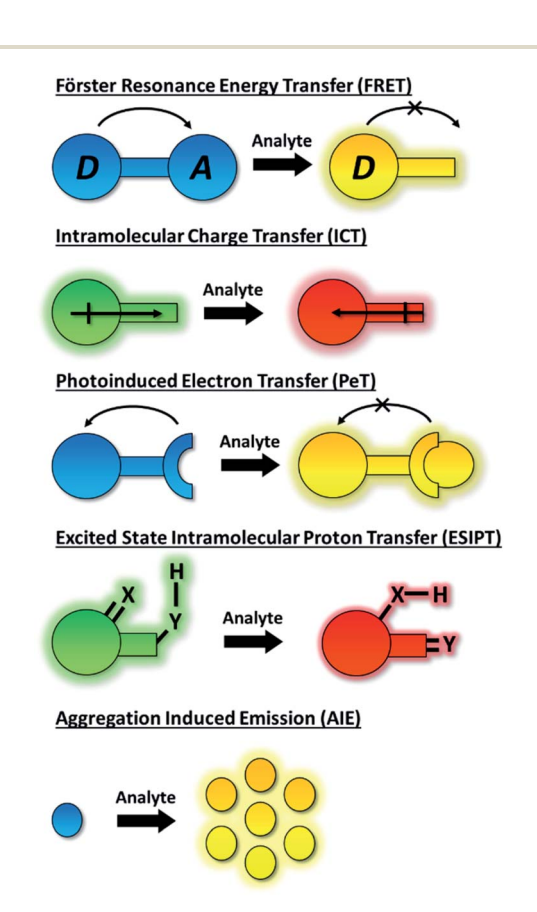
Xue Tian, $^{\boxed{\tiny \dag}}$ † Lloyd C. Murfin, $^{\boxed{\tiny \dag}}$ † Luling Wu, $^{\boxed{\tiny \dag}}$ Simon E. Lewis $^{\boxed{\tiny \dag}}$ and Tony D. James $^{\boxed{\tiny \dag}}$

Small-molecule based fluorescent probes are increasingly important for the detection and imaging of biological signaling molecules due to their simplicity, high selectivity and sensitivity, whilst being non-invasive, and suitable for real-time analysis of living systems. With this perspective we highlight sensing mechanisms including Förster resonance energy transfer (FRET), intramolecular charge transfer (ICT), photoinduced electron transfer (PeT), excited state intramolecular proton transfer (ESIPT), aggregation induced emission (AIE) and multiple modality fluorescence approaches including dual/triple sensing mechanisms (DSM or TSM). Throughout the perspective we highlight the remaining challenges and suggest potential directions for development towards improved small-molecule fluorescent probes suitable for biosensing.

Introduction

The dynamic chemical diversity of the numerous elements, ions and molecules that constitute the basis of life provides wide challenges and opportunities for research. Due to their high levels of sensitivity, fast response time, and technical simplicity, small molecule based fluorescent probes have been widely developed and applied to the detection of many biologically important analytes. 1-10 In particular, fluorescent probes for biologically and/or environmentally important cations, anions, small neutral molecules, and biological macromolecules (such as protein and DNA) have been developed to complement the rapid development of microscopic imaging technologies. As such, fluorescent probes have been extensively used in diverse fields such as biology, physiology, medicine, pharmacology, and environmental sciences. Such probes exhibit changes in fluorescence intensities or emission wavelengths through one or more sensing mechanisms, including Förster resonance energy transfer (FRET),11 intramolecular charge transfer (ICT),1 photoinduced electron transfer (PeT),12 excited state intramolecular proton transfer (ESIPT),13 aggregation induced emission (AIE),14,15 or involve dual/triple sensing mechanisms (DSM or TSM) (Scheme 1).16 Importantly, the number of fluorescence based systems continues to expand exponentially, in order to keep pace with the ever expanding fluorescence imaging modalities, including super-resolution-based technologies such as Stochastic Optical Reconstruction Microscopy (STORM),17 PALM (photoactivated localization microscopy)18 and super-resolution photoacoustic imaging (PAI). 19-21

An ideal fluorescence sensing system provides a reliable output response under analytical conditions which relates directly to the concentration of the analyte present. Such



Scheme 1 Schematic representation of the fluorescent mechanisms discussed in this perspective.

[&]quot;Department of Chemistry, University of Bath, Bath, BA2 7AY, UK. E-mail: lw960@bath.ac.uk; s.e.lewis@bath.ac.uk; t.d.james@bath.ac.uk

^bSchool of Chemistry and Chemical Engineering, Henan Normal University, Xinxiang 453007, P. R. China

[†] The first two authors contributed equally to this work.

interactions can be reversible (the probe being described as a "chemosensor") providing an accurate reflection of analyte concentration that may change over time. If the interaction process is irreversible (the probe being given the term "chemodosimeter") the response will indicate only the maximum concentration of analyte present. Importantly, for fluorescent systems, the nature of the probe's response can also vary. In particular a turn-on fluorescence response upon analyte detection is desired, to differentiate the response from environmental quenching effects. Likewise, the use of turn on/off fluorescent probes that exhibit only a single emission maximum for quantifying target analytes may be fraught with difficulties due to interference from various analytically unrelated factors. Instruments' parameters, the microenvironment around the probe molecule, etc. can all interfere with the analysis.22 Significantly, by taking the advantage of the ratiometric approach these problems can be successfully overcome. The ratiometric fluorescence response depends on the intensity change of two or more emission bands of a probe species before and after the analyte recognition event. As such, it provides an effective internal reference that significantly improves sensitivity and quantification.

Amongst organic fluorescent probes, near-infrared (NIR, 650-900 nm) probes have proven to be especially advantageous when used in vivo or in vitro.23-26 Such probes allow for deeptissue penetration, reduce interference from haemoglobin and water,27 and lessen the risk of photobleaching due to the lower energy of excitation required.²⁸ Furthermore, autofluorescence of endogenous species is reduced since such species usually absorb or emit below 600 nm.29 The use of two-photon (TP) excitation, first described by Webb et al. in 1990,30 has been widespread in the world of NIR fluorescent probes.31,32 TP excitation occurs when two (typically NIR) photons of similar energy are absorbed by a molecule, and the combined energies promote it to an excited state suitable for fluorescence emission.33 TP fluorescence has the same advantages as NIR fluorescence, but in addition can generate fluorescence emissions in the visible region. Furthermore, it allows for specific localisation of excitation, since the absorption of two photons only happens within the focal plane, therefore potentially reducing photodamage.34 However, some evidence suggests that use of TPM for biological imaging can in fact lead to greater photobleaching (in comparison to single photon experiments), dependent on the power level at which the imaging is performed.35 However, the extent of photobleaching can be minimised by use of higher pulse repetition rates in preference to a continuous laser source.36

In this perspective, we will highlight the features of fluorescent probes that use a variety of different fluorescence mechanisms, with a focus on those that have shown promise in the realms of biological sensing and imaging. Moreover, we will highlight how fluorescent probes with optimized optical properties are powerful tools for biological research. For example, NIR emission and TP probes are useful to image target analytes in deep tissues. After detailing prominent examples using each fluorescence technique, a consideration of the advantages and disadvantages of that mode of fluorescence is also presented.

Förster resonance energy transfer (FRET) probes

Förster resonance energy transfer (FRET) is a non-radiative process in which excited dye donors transfer energy to ground state dye acceptors through a long range dipole-dipole interaction (Fig. 1).37 The donor moiety absorbs higher energy, shorter wavelength light, whereas the acceptor absorbs and emits lower energy, longer wavelength light. Considerations for designing FRET-based probes include: (1) the donor-acceptor pair should be within 10-100 Å of each other, (2) emission spectrum of the donor and the absorption spectrum of the acceptor should overlap, (3) donor emission moment, acceptor absorption moment, and the separation vector should be favourably oriented. At this point readers are directed to a recent review by James et al. covering FRET-based smallmolecule fluorescent probes for the detection or imaging of cations, anions, small neutral molecules, biomacromolecules, cellular microenvironments and dual/multi-analyte responsive systems.11

Han et al. have developed a ratiometric probe ThioRB-FITC-MSN for sensing lysosomal hypochlorous acid (HOCl).³⁸ The probe is composed of silica nanoparticles with a fluorescein fluorophore as the donor dye and a non-fluorescent spirothioether unit which reacts with HOCl to generate a fluorescent rhodamine as the acceptor dye. ThioRB-FITC-MSN has an emission maximum at $\lambda_{\rm em} = 526$ nm ($\lambda_{\rm ex} = 490$ nm). In the presence of HOCl, an increase in emission at $\lambda_{em} = 586$ nm accompanied by decreased emission at $\lambda_{\rm em} = 526$ nm occurs, which was attributed to the HOCl-triggered tandem oxidation and β-elimination of the spirothioether-bearing unit to produce rhodamine, facilitating FRET from the fluorescein donor to the rhodamine acceptor and emission at $\lambda_{em} = 586$ nm (Scheme 2). ThioRB-FITC-MSN exhibited good selectivity towards HOCl over

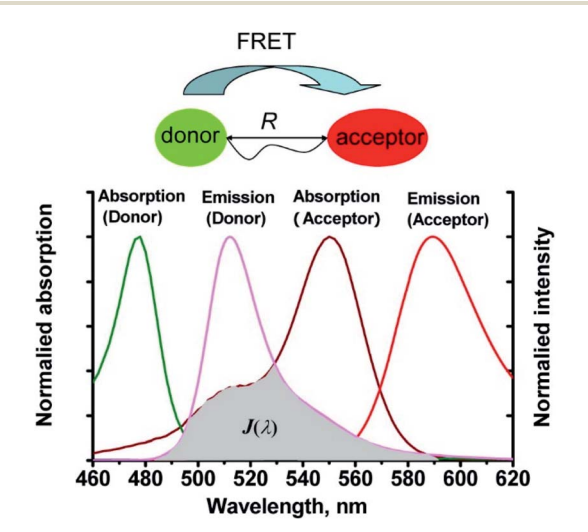


Fig. 1 The mechanism of Förster resonance energy transfer (FRET). R is the distance between the energy donor and acceptor, $J(\lambda)$ represents the degree of spectroscopic overlap between the donor emission and the acceptor absorption. Reproduced with permission from ref. 37. Copyright 2013, American Chemical Society.

Scheme 2 FRET-based ratiometric fluorescent probe ThioRB-FITC-MSN for the detection of HOCL.

other reactive oxygen and nitrogen species (ROS/RNS) including nitric oxide (NO), $\rm H_2O_2$, 'OH, ROO' or $\rm O_2$." Furthermore, after L929 cells were stained with **ThioRB-FITC-MSN** and Lyso-Tracker Blue DND-22 (a lysosome marker), L929 cells exhibited excellent fluorescence co-localisation of the probe and Lyso-Tracker Blue, which indicated that **ThioRB-FITC-MSN** was suitable for targeting the lysosomes of L929 cells.

Qian *et al.* have developed a FRET-based small molecule fluorescent probe **PNCy3Cy5** for the selective detection of peroxynitrite (ONOO⁻) in living cells.³⁹ The cyanine dyes Cy3 and Cy5 are bright and photostable, and are well suited for the fluorescence imaging of living cells. **PNCy3Cy5** contains a Cy3 and Cy5 dyad which serves as the fluorescence energy donor and acceptor pair separated by an acetyl–piperazinyl–hexanoyl spacer that tethers the Cy3 and Cy5 together (Scheme 3). **PNCy3Cy5** displays fluorescence emission for Cy5 ($\lambda_{\rm ex}$ =

PNCy3Cy5

PF6

ONOO

FRET off

PNCy3

PNCy3

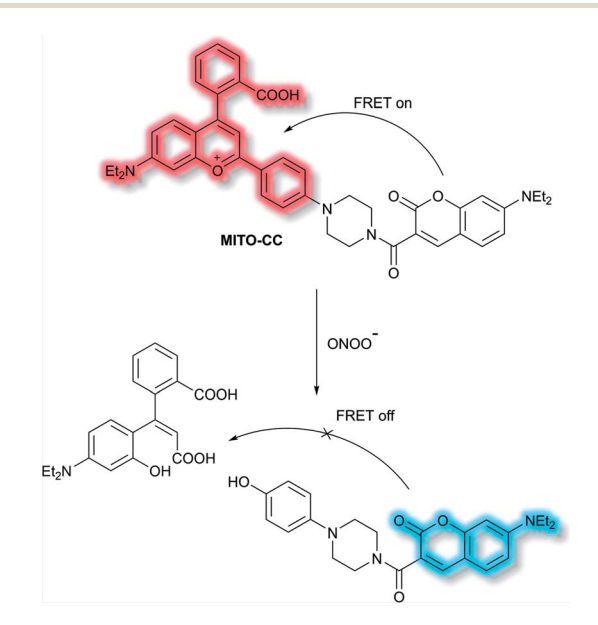
PNCy3

Scheme 3 Cy3 and Cy5 (energy donor and acceptor)-based FRET fluorescent probe PNCy3Cy5, developed for the ratiometric detection of ONOO⁻. Also shown is the structure of its cleavage product PNCy3.

530 nm, $\lambda_{\rm em}=660$ nm) due to FRET from Cy3. However, in the presence of ONOO⁻, the Cy5 moiety was selectively oxidised to its oxindole derivative, terminating the FRET process, resulting in a fluorescence increase at $\lambda_{\rm em}=560$ nm and a decrease at $\lambda_{\rm em}=660$ nm, the fluorescence intensity ratio $I_{560\rm nm}/I_{660\rm nm}$ displaying a nearly 324-fold enhancement. The proposed cleavage-based mechanism of action was supported by mass spectrometric analyses, which confirmed the formation of the oxidized product **PNCy3**. Furthermore, **PNCy3Cy5** exhibits an excellent detection limit of 0.65 nM and high detection selectivity in 0.1 M phosphate buffer (0.2% DMF, v/v, pH = 7.4). Inspired by these results, **PNCy3Cy5** was used as a ratiometric sensor for both exogenous and endogenous fluorescence imaging of ONOO⁻ in RAW264.7 macrophages.

Chang *et al.* have reported a TP ratiometric fluorescent probe MITO-CC based on FRET for the detection of mitochondrial ONOO⁻. MITO-CC combined a modified chromenylium fluorophore as the energy acceptor and a modified coumarin as the energy donor (Scheme 4). In the absence of ONOO $^-$, MITO-CC exhibited a strong emission at 651 nm and a weak emission of coumarin at 473 nm. Upon addition of ONOO $^-$ (0 to 7.5 μ M), a 93-fold fluorescence ratio (I_{473 nm/ I_{651} nm) enhancement was reported. Furthermore, a low limit of detection (LoD, 11.3 nM), fast response (less than 20 s) and high selectivity over other biological ROS/RNS including NO, NO2 $^-$, H₂S, H₂S₂, HNO, H₂O₂ and HOCl in PBS buffer solution (25 mM, containing 30% ethanol, pH 7.4) were observed. Moreover, the low cytotoxicity of MITO-CC facilitated the monitoring of endogenous ONOO $^-$ in HepG2/RAW264.7 cells and an LPS-stimulated mouse model.

Chang *et al.* have developed a novel FRET-based ratiometric fluorescent probe **FIP-1** for the detection of ferrous cation (Fe²⁺) in living systems. ⁴¹ **FIP-1** links a 5-aminomethyl fluorescein (5-AMF) donor and a cyanine 3 (Cy3) acceptor through an endoperoxide bridge as a Fe²⁺ responsive trigger (Scheme 5). The



Scheme 4 FRET-based ratiometric fluorescent probe **MITO-CC** for the detection of ONOO⁻.

Perspective **Chemical Science**

Scheme 5 FRET-based ratiometric fluorescent probe FIP-1 for the detection of Fe²⁺

initial state of probe FIP-1 is FRET on, with emissions at 515 nm and 556 nm, when excited at 488 nm. However, with the addition of Fe²⁺ the endoperoxide core can be cleaved, which leads to dissociation of the donor and acceptor, resulting in FRET turn off. This leads to increased emission at 515 nm and loss at emission at 556 nm, corresponding to the emission of the 5-AMF donor. FIP-1 exhibited high selectivity and sensitivity towards Fe²⁺ over other competing biologically relevant metals such as Fe³⁺, Cu²⁺ and Zn²⁺, facilitating the imaging of labile iron pools in HEK 293T cells.

Reactive sulfur species (RSS) have become an important research area due to their vital physiological functions. Among the RSS, hydrogen sulfide (H₂S) is perhaps the most attractive to study, since changes in H2S metabolism can lead to an array of pathological disturbances in the form of hypertension, atherosclerosis, heart failure, and diabetes. 42,43 In 2019, Zhang et al. developed a single dual-reactive FRET-based fluorescent probe N₃-CR-PO₄ for monitoring how phosphatase activity depends on the levels of H2S in cells. The FRET system consists of an N3modified coumarin and phosphate-modified rhodol, connected by a piperazine bridge.44 The proposed sensing mechanism is depicted in Scheme 6. Initially, N3-CR-PO4 exhibits relatively weak fluorescence peaks at 445 and 545 nm upon excitation at 360 nm in Tris-HCl buffer (pH 7.2). However, upon addition of H_2S , a blue fluorescence at $\lambda_{em}=445$ nm ($\lambda_{ex}=360$ nm) was observed due to the reduction of the -N3 to -NH2. Subsequently, on the addition of alkaline phosphatase (ALP), the phosphate group of N₃-CR-PO₄ was cleaved, leading to recovery of the green fluorescence at $\lambda_{em} = 545 \text{ nm} (\lambda_{ex} = 510 \text{ nm})$ of rhodol in Tris-HCl buffer (pH 8.0). In the presence of fixed concentrations of H₂S followed by addition of ALP, the fluorescence at λ_{em} = 445 nm decreased gradually, and the fluorescence at $\lambda_{\rm em}$ = 545 nm significantly increased, due to FRET from the donor (coumarin) to the acceptor (rhodol). Furthermore, N3-CR-PO4 was shown to have high selectivity for ALP over other enzymes, amino acids, proteins, peptides, and inorganic salts. Importantly, it was confirmed in HeLa cells that intracellular concentrations of H₂S exhibited a crucial role in regulating the activity of the phosphatase enzyme. It was found that cells can regulate their H₂S concentrations in order to maintain an optimal level of phosphatase activity.

β-Secretase (BACE1) is an important enzyme in Alzheimer's disease (AD).45 β-amyloid (Aβ) peptides are generated by sequential cleavages from BACE1, and the accumulation of AB is

Scheme 6 FRET-based N₃-CR-PO₄ developed for the detection of H₂S and phosphatase.

2hv

BACE1

mCyd

AF633

Chemical Science

Scheme 7 Illustration for the working principle of the designed TP ratiometric fluorescent probe AF633mCyd, for the determination of BACE1 in neurons and mouse brain tissue slice. Reproduced with permission from ref. 47. Copyright 2020, The Royal Society of Chemistry.

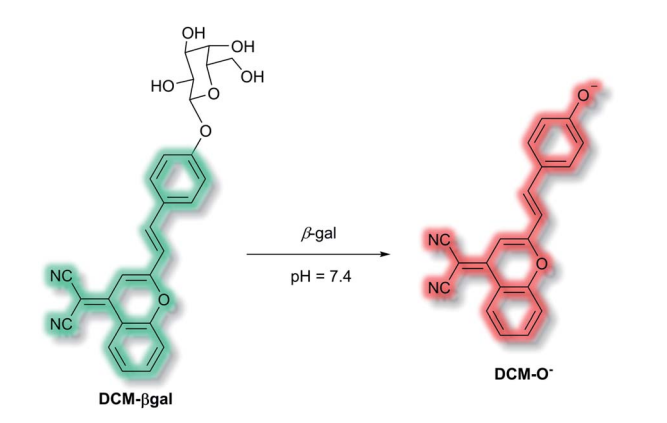
responsible for the pathogenesis of AD.46 Recently, Tian and colleagues have created a FRET-based TP ratiometric fluorescent probe AF633mCyd for the bioimaging and sensing of BACE1 in different regions of AD mouse brain. The FRET system contains an acceptor - Alexa Fluor 633 (AF633) and a donor merocyanine derivative (mCyd) which are connected by a linker that is a substrate of the enzyme, with a chain length less than 10 nm, as shown in Scheme 7.47 The peptide substrate (EVNL-DAEFRHDSGYK) was inserted between the donor and acceptor, then because the linker can be specifically cleaved by BACE1 the donor and acceptor are separated. The sensing mechanism was confirmed using mass spectrometry. AF633m-Cyd exhibited a maximum emission at 651 nm upon TP excitation at 820 nm, which was ascribed to the emission profile of the fluorescent acceptor AF633. Exposure of AF633mCvd to BACE1 results in the separation of the donor and acceptor in this system which caused a reduction in the AF633-based fluorescence emission at 651 nm and an increase in mCyd-based fluorescence emission at 578 nm. Importantly, AF633mCyd displayed high selectivity and sensitivity, as well as good biocompatibility and long-term stability, facilitating its application for the bioimaging and sensing of BACE1 in live neurons and different regions of AD mice brains. The fluorescence emission ratio of AF633mCyd displayed good linearity with concentrations of BACE1 from 0.1 to 40.0 nM providing a LoD of 65.3 ± 0.1 pM (fresh cell lysates containing 0.05% DMSO, pH 4.5).

FRET-based fluorescent probes are widely used to monitor cellular dynamics in living cells in real time. Advantages of FRET-based fluorescent probes include large Stokes shifts, ratiometric sensing, and dual/multi-analyte responsive systems. Despite the value of these characteristics, the applicability of FRET is still dependent on the FRET efficiency; the distance between the donor and acceptor moieties strongly influences the efficiency of FRET. Therefore, this technology still requires further investigation and development. For instance, combining FRET with advanced fluorescence microscopy techniques, such as fluorescence lifetime imaging microscopy (FRET-FLIM), offers a sensitive method for lifetime measurements. Between the donor and acceptor moieties strongly influences the efficiency of FRET with advanced fluorescence microscopy techniques, such as fluorescence lifetime imaging microscopy (FRET-FLIM), offers a sensitive method for lifetime measurements.

3. Intramolecular charge transfer (ICT) probes

A common approach for analyte detection is the use of intramolecular (or internal) charge transfer (ICT) probes. Fluorophores of ICT probes are made of 3 conjugated parts - an electron donor (D), an electron acceptor (A) and π -conjugated linker.1 When ICT probes interact with the desired analyte, the electron density in the recognition group is altered (e.g. as a result of bond cleavage, substitution, or substrate coordination) which installs a 'push-pull' system in the molecule. Excitation of the resultant species, in tandem with the altered electron distribution, affords a large dipole and altered excited state to that of the initial probe.49 As such, ICT probes commonly exhibit a 'turn-on' fluorescence response and wavelength shift of the fluorescence after interaction/recognition of the analyte (though there key instances where ICT probes allow for a ratiometric analysis, where instead a shift of the fluorescence response is given).50,51

Use of ICT probes is particularly prevalent for detecting enzyme activity, especially when coupled with the advantages of NIR fluorescence (e.g. deep tissue penetration, low background fluorescence).52 In 2016, Zhu et al. reported an in vivo NIR probe to target enzyme β -galactosidase (β -gal), a biomarker for cell senescence and primary ovarian cancers.53 The probe, DCM- β gal, was composed of a dicyanomethylene-4*H*-pyran (**DCM**) NIR fluorophore connected to a sugar recognition moiety. Initial evaluation using PBS/DMSO indicated that in the presence of β -gal, the sugar moiety of **DCM**- β gal could be cleaved to release DCM-O (Scheme 8). The process was found produce a ratiometric ($\lambda_{ex} = 450$ nm, $\lambda_{em} = 685$ nm and 500 nm) and turn-on ($\lambda_{\rm ex} = 535$ nm, $\lambda_{\rm em} = 685$ nm) fluorescence response depending on the excitation wavelength. The response of DCM- β gal towards β -gal was rapid, with a plateau in fluorescence after 35 minutes. A detection limit of $1.7 \times 10^{-4} \text{ U mL}^{-1}$ was obtained. DCM- β gal was highly selective towards β -gal over other enzymes (cellulase, reductase, lysozyme, esterase) and biologically relevant species (Cys, Hcy, GSH, H2O2, H2S, dithiothreitol). DCM-βgal could be used to visualise 293T (human embryonic kidney) cells. Specifically, 293T cells with



Scheme 8 Detection mechanism of probe DCM- β gal towards β -gal.

the lacZ gene (i.e., over expressing β -gal) resulted in a fluorescence decrease of the green channel ($\lambda_{\rm em}=490\text{-}530$ nm) and increase in the red channel ($\lambda_{\rm em}=650\text{-}720$ nm). Conversely, 293T cells lacking lacZ displayed fluorescence predominantly in the green channel over the red channel. A 5-fold increase in the ratiometric fluorescent response was measured when the lacZ gene was present. Finally, **DCM-\betagal** was evaluated in tumourbearing mice; fluorescence was observed within 5 minutes of **DCM-\betagal** injection. This work reports the first real-time $in\ vivo$ 3D imaging of β -gal.

A family of enzymes that have received significant attention are the cytochrome P450 (CYP) enzymes. 54,55 In 2019, Ma et al. described a probe to determine the catalytic activity of CYP450, and in particular the isoform CYP2J2, a potential cancer biomarker involved in cell proliferation, angiogenesis, and metastasis.56,57 Like CYP1A, CYP2J2 effects o-dealkylation of its substrates. The HXPI fluorophore was selected based on its good tissue penetration, low cytotoxicity, and the flexibility of the molecule favouring binding in the active site of CYP2J2. Initial screening of the recognition moieties indicated that omethylated HXPI, MXPI, was able to fit the active site of CYP2J2, but metabolism of the recognition group was low. Addition of the self-immolative p-hydroxybenzyl (PHB) linker was found to increase metabolism of the probe. In silico studies rationalised this as being due to the placement of the OMe group closer to the catalytic site of CYP2J2. Screening a series of o-alkyl recognition moieties found that o-methylation was optimal, overall affording BnXPI (Scheme 9). In PBS solution (pH 7.4), BnXPI exhibited a turn-on fluorescent response towards CYP2J2 (λ_{ex} = 656 nm, $\lambda_{em} = 718$ nm), and was found to be highly selective (46-fold) towards CYP2J2 (detection limit of 0.024 mg mL⁻¹) when compared to other CYP isoforms. Testing of BnXPI in HLMs showed that the probe could successfully monitor CYP2J2 activity with calculated metabolic rates comparable to those of determined using the nonfluorescent standard astemizole. NIR fluorescence bioimaging of CYP2J2 in cells was achieved in a range of human cancer cell lines (U251, HepG2, A549, and K562) within 1 h at physiological pH ($\lambda_{ex} = 633$ nm, $\lambda_{\rm em} = 690\text{--}750$ nm). Exogenous inhibition of CYP2J2 confirmed the observed fluorescent enhancements were afforded by CYP2J2. Furthermore, BnXPI was shown to detect angiogenesis in human umbilical vein endothelial cells (HUVEC) in vivo and ex vivo; significant fluorescent enhancement was achieved and neovessel growth could be followed due to the increased

expression of CYP2J2 in such environments. In addition, **BnXPI** could be used as a clinical tool for patients with cancer. In healthy patients, peripheral blood samples treated with **BnXPI** showed little fluorescence response. Conversely, samples taken from lymphoma and leukaemia patients showed significant fluorescent turn-on response, which was found to be proportional to expression of CYP2J2. Finally, it was shown that **BnXPI** could be used for real-time *in vivo* imaging of tumours in mice. Injection with **BnXPI** afforded both a rapid (<10 min) and selective fluorescence response localised within the tumour region.

Another area in which NIR ICT probes have been used is in the detection of (non-peptidic) biologically relevant small molecules. One such class of analytes are reactive oxygen species (ROS), which are associated with oxidative stress and as a result received much attention in the world of fluorescent probes for biological applications. 58,59 In 2019, a TP fluorescent probe for the detection of the ROS hydroxyl radical ('OH) was developed by Tang et al.60 It is known that 'OH can cause oxidative damage, which has been suggested to contribute to the pathogenesis of depression. The authors proposed that live monitoring of 'OH in the brain is key to understanding this relationship, and of all the bioimaging tools two photon microscopy (TPM) would be the most advantageous. Probe MD-B incorporated a courmarin 151 (Cou151) fluorophore due to its known TP properties, large Stokes shift, and ICT character. A pyrazolone was employed as a recognition group for 'OH, in which the electron donor ability of the anilinic nitrogen incorporated into the pyrazolone system is attenuated, thereby masking the inherent ICT system of Cou151. The initial OP (λ_{ex} = 370 nm, $\lambda_{\rm em}$ = 500 nm) and TP ($\lambda_{\rm ex}$ = 800 nm, $\lambda_{\rm em}$ = 500 nm) experiments in PBS-buffer (pH 7.4) indicated that MD-B exhibits a significant turn-on fluorescence response, which scaled linearly with 'OH. It was proposed that the turn-on response upon addition of 'OH was caused by a single-electron oxidation of MD-B to form fluorescent species MD-B-OH, in which the Cou151 ICT system is restored (Scheme 10). An increase in quantum yield ($\varphi_f = 0.037$ to $\varphi_f = 0.25$ for MD-B and MD-B-OH respectively) and in TP action cross section ($\sigma = 5.0$ GM to $\sigma =$ 42.6 GM) was observed. MD-B was also found to selectively detect 'OH over all other ROS tested, including O2'-, H2O2, TBHP, OCl⁻, ¹O₂, NO, ONOO⁻, 2,2'-azobisisobutyronitrile (AIBN), 2,2'-azobis(2,4-dimethylvaleronitrile) (AMVN), and CO3'-. A detection limit for MD-B towards 'OH was determined

Scheme 9 Mechanism of detection of CYP2J2 by probe BnXPI, with initial test compound MXPI and fluorophore OXPI (deprotonated HXPI) also shown.

Chemical Science Perspective

Scheme 10 Detection of 'OH with ICT probe MD-B

as 2.4 nM. MD-B was successfully employed to detect 'OH in human astrocytes pre-treated with the 'OH inducer glutamate, in PC12 cells, and in mouse RAW 264.7 cells by TP fluorescence ($\lambda_{\rm em} = 400$ –650 nm). Furthermore, human astrocytes treated with the 'OH scavenger mannitol, as well as glutamate, saw a significantly decreased fluorescence response. MD-B was shown to be able to cross the blood-brain barrier and to detect 'OH in the brains of mice under the stress of restraint. Furthermore, MD-B could actively monitor fluctuating levels of 'OH in mice with depression-like behaviour - mice exposed to chronic unpredictable mild stress (CUMS). Remarkably, TP images of the brains of CUMS mice indicated a significant (6fold) turn-on fluorescence in contrast to control mice. It was hypothesised that MD-B could be used to evaluate the connection between 'OH and SIRT1, an acetylase enzyme associated with depression. Through a combination of 'OH inhibition and induction experiments in human astrocytes, it was confirmed that SIRT1 activity was reduced by 'OH. Furthermore, LC-MS/ MS proteomic analysis indicated that 'OH oxidises the phenylalanine residues in the active site of SIRT1, thereby reducing its activity. From these results the authors suggested that 'OH, due to its role in stress and SIRT1, must play an important role in depression.

Also in 2019, Lewis et al. reported an azulene probe for detection and imaging of ROS, the first probe employing an azulene fluorophore for fluorescence microscopy.⁶¹ Here, the Bpin group was chosen as the receptor motif due to its high affinity and selectivity for ONOO-.62 It was proposed that upon addition of ONOO-, and reaction to give the corresponding alcohol, the electron-donating -OH group would reinforce the inherent polarity of the azulene core via an ICT mechanism and in doing so cause a turn-on fluorescence response. Ethyl esters were incorporated at the 1- and 3-positions to increase the stability of the probe, overall affording AzuFluor® 483-Bpin. Upon reaction with H2O2, AzuFluor® 483-Bpin was rapidly converted to 6-hydroxy species 1 (Scheme 11). As expected, AzuFluor® 483-Bpin, was found to be non-fluorescent, but underwent a significant fluorescent turn-on in the presence of ROS as 1 is formed ($\lambda_{\rm ex} = 350$ nm, $\lambda_{\rm em} = 483$ nm). As expected AzuFluor® 483-Bpin was found to be highly selective towards ONOO over other ROS at equivalent concentrations, but also exhibited a response to H₂O₂ at higher concentrations. Emission at $\lambda_{em} = 483$ nm was enhanced with increasing [ONOO⁻] or $[H_2O_2]$, with detection limits calculated to be 21.7 nM and 1.72

Scheme 11 Detection of ROS with TP ICT probe AzuFluor® 483-Bpin.

μM respectively. AzuFluor® 483-Bpin was then evaluated as a TP chemodosimeter for ROS. The maximum TP fluorescence emission was observed at 700 nm for AzuFluor® 483-Bpin, which upon addition of ONOO was found to shift to 810 nm. At 810 nm, the TP action cross-section of **1** was found to be $\sigma = 3.2$ GM. In vitro HeLa cell studies indicated that when excited at 800 nm, the emission intensity of AzuFluor® 483-Bpin + ONOO increased 4-fold in respect to AzuFluor® 483-Bpin. The probe was also shown to successfully undergo turn on fluorescence, and subsequent TPM imaging, of RAW 264.7 cells pretreated with inducers of endogenous ROS. Both induction and inhibition studies confirmed the fluorescence response was due to the interaction of AzuFluor® 483-Bpin and ROS. Finally, AzuFluor® 483-Bpin was used to successfully image endogenous ONOO and H2O2 in rat hippocampal tissue via TP microscopy (TPM, $\lambda_{ex} = 800$ nm, $\lambda_{em} = 400-600$ nm), demonstrating that AzuFluor® 483-Bpin can detect ROS in tissue.

A class of biomolecules often studied in tandem with ROS are biothiols, which commonly act as antioxidants in many biological systems, as well as being associated with various disease states (e.g., Alzheimer's disease, liver damage). In 2016, Lin et al. published an NIR probe able to detect and image biothiols at both high and low concentrations. 63 It was proposed that use of a single probe with 2 distinct chemical handles would allow for the detection of multiple biothiol species that would otherwise require multiple probes, avoiding any associated issues (e.g. fluorescence cross talk, localisation issues). The probe CHMC-Thiol consisted of chlorohydroxylmerocyanine (CHMC) NIR fluorophore and uses two thiol recognition units. receptor has either 'high-sensitivity' trobenzenesulfonate) or 'low-sensitivity' (chloride) towards thiols.

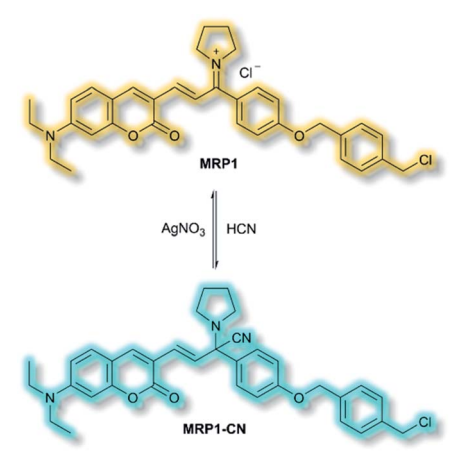
CHMC-Thiol is non-fluorescent, but upon addition of low concentrations of Cys (0-50 µM, 0-10 eq.) a turn-on fluorescence response was observed ($\lambda_{ex} = 550$ nm, $\lambda_{em} = 680$ nm). When CHMC-Thiol was combined with increasing concentrations of Cys (50-500 µM, 10-100 eq.) a ratiometric fluorescent response was observed ($\lambda_{\rm em} = I_{\rm 625nm}/I_{\rm 680nm}$). It was proposed that at low concentrations, Cys attacks the CHMC-Thiol at the 'high-sensitivity' sulfonate group to generate the corresponding fluorescent species CHMC1, in which the liberated phenol moiety creates an ICT system (Scheme 12). Reaction of CHMC-Thiol with higher concentrations of Cys effects both cleavage of the 'high-sensitivity' recognition moiety, and in addition substitution of the 'low-sensitivity' chloro group attached to the CHMC core. Initial attack of the thiol in Cys generates intermediate 2 in which Cys is S-linked to the CHMC core, which

Perspective **Chemical Science**

Scheme 12 High and low concentration of Cys detection pathways of probe CHMC-Thiol

undergoes an intramolecular addition-elimination reaction to afford N-linked 3. CHMC-Thiol could be used to detect Hcy and GSH. CHMC-Thiol reacts with Hcy to induce a fluorescence response analogous to the reaction with Cys. While with GSH, at low concentrations a turn-on fluorescence at $\lambda_{\rm em} = 680$ nm was observed, but at higher concentrations only the thioether product was formed, and no intramolecular addition/ elimination occurs. This resulted in a 10 nm redshift (λ_{em} = 690 nm) in fluorescence emission. The selectivity of CHMC-**Thiol** at both $\lambda_{em} = 680$ nm and $\lambda_{em} = 625$ nm was determined. As expected, the probe exhibited a response towards GSH, Hcy, and Cys at 680 nm. A mild response was also elicited with Na₂S. All other analytes tested (metal cations, ROS, RNS, and biological anions) did not generate a fluorescence response. Conversely, at 625 nm a fluorescent response was only observed for Cys and Hcy. CHMC-Thiol was then evaluated in living cells. A strong fluorescence response was observed in the red channel $(\lambda_{\rm em} = 650-750 \text{ nm})$ for HeLa cells incubated with CHMC-Thiol. Furthermore, cells treated with exogenous Cys exhibited significant fluorescence enhancement in the orange channel $(\lambda_{\rm em} = 580\text{-}640 \text{ nm})$, as well as fluorescence in the red channel. From these observations, the authors concluded that CHMC-Thiol gave a turn-on response at low Cys concentrations, and a ratiometric response at high Cys concentrations. Analogous results were obtained from imaging experiments using Kunming mice.

The final probe to be discussed in this section is the mitochondria-specific HCN probe developed by Sessler et al. in 2018.64 Whilst HCN is a well-recognized toxin, endogenous HCN is thought to play a physiological role within neurons. The probe MRP1 was designed using the diethylaminocoumarin ICT fluorophore and a methylenepyrrolidinium recognition unit. Addition of a para-alkoxy group increased the φ_f and a benzyl chloride group was included to immobilise MRP1 within mitochondria by reacting with protein thiols. The recognition unit of MRP1 was found to react with HCN both reversibly and rapidly to give MRP1-CN, exploiting the nucleophilicity of the cyanide anion at physiological pH (Scheme 13). In solution (PBS/MeCN, 1:3, v/v, pH 7.4), MRP1 exhibited an a linear,



Scheme 13 Reversible detection of HCN of ICT probe MRP1

ratiometric fluorescence response ($\lambda_{\rm ex} = 467$ nm, $\lambda_{\rm em} = I_{490{\rm nm}}$ / $I_{599\mathrm{nm}}$) upon addition of cyanide, and a detection limit of 65.6 nM. The probe was stable for over 24 h in solution, whilst time trial experiments indicated the detection of KCN in <1 s. MRP1 was selective towards cyanide over other relevant anions (e.g. halides, acetate, sulfate, nitrate, perchlorate and azide). Furthermore, the probe could be cycled 'on' and 'off' repeatedly by sequential addition of cyanide and AgNO₃ respectively.

Colocalization experiments with Mitotracker Deep Red indicated that MRP1 localised in cell mitochondria, with a Pearson's colocalization coefficient of 0.94. Importantly, it was retained in mitochondria after the membrane potential was destroyed. HepG2 cells incubated with only MRP1 gave no fluorescence in the green channel ($\lambda_{\rm em} = 460$ –530 nm), but strong emission in the red channel ($\lambda_{em} = 575-650$ nm). Upon addition of KCN, fluorescence enhancement of the green channel was observed alongside reduced emission in the red channel. The green-to-red ratiometric response scaled linearly when KCN was added. Endogenous HCN studies were performed with neuron-like rat pheochromocytoma cells due to their natural production of HCN. Within 15 minutes of addition of MRP1, a strong emission was observed in the green channel and weak emission in the red channel. A combination of cyanide stimulation with hydromorphine and quenching with methemoglobin confirmed that the ratiometric response was due to endogenous HCN production. Sequential use of hydromorphine and methemoglobin indicated that MRP1 was able to dynamically respond to changing HCN concentrations. It should be noted that this is the first example of a fluorescent HCN probe capable of monitoring endogenous HCN.

ICT probes are often simple in design, allowing for straightforward syntheses and clear mechanisms of action upon formation of the D- π -A system. Once a clear a mechanism of detection is established (e.g. a turn-on fluorescence response or a ratiometric response), the recognition moieties of ICT probes can often be easily substituted for those that detect other species of interest. As such, ICT systems often provide straightforward routes to a family of probes for an array of analytes. The main limitations of ICT probes are due to the risk

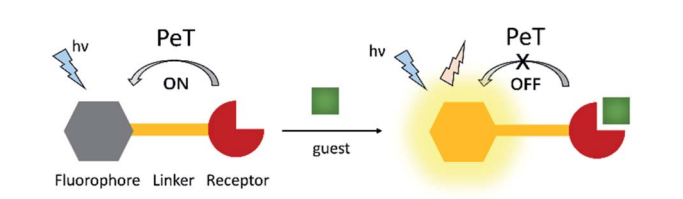
Chemical Science Perspective

of reduced fluorescence as a result of aggregate-caused quenching (ACO), and that the nature of their fluorescence is dependent on the solvent in which the experiments are performed (due to the corresponding solute-solvate interactions).65 The second of these issues can often lead to problems when results from initial organic-solvent based experiments are not reproducible in *in vitro* studies in biological media (*i.e.* buffered aqueous solutions). Furthermore, the broad emissions often exhibited by ICT fluorophores can prove troublesome when the fluorophore exhibits a ratiometric response.66

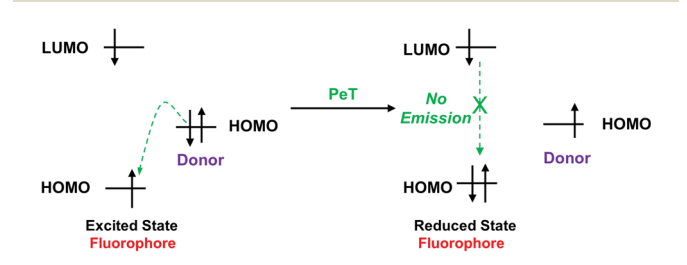
Photoinduced electron transfer (PeT) probes

Photoinduced electron transfer (PeT) is one of the most important mechanisms for developing fluorescent probes and biosensors. The phenomenon of PeT was first described in the 1970s.67,68 With PeT systems, the intramolecular transfer of electrons from the receptor to the fluorophore results in fluorescence quenching. However, when the receptor binds to its target, the PeT process is inhibited or completely suppressed, which means the sensor restores its fluorescence (Scheme 14).69 PeT based fluorescence probes usually have "turn on" features, which are conducive to fluorescence imaging with high signalto-noise ratios.

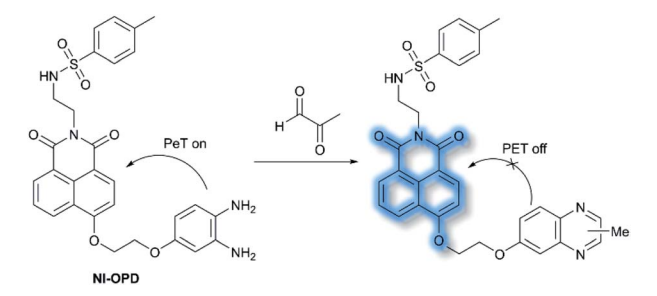
When a fluorophore is excited by an appropriate wavelength of light, an electron from the highest occupied molecular orbital (HOMO) is transferred to the lowest unoccupied molecular orbital (LUMO). If the energy level of the HOMO of the adjacent receptor group lies between the LUMO and HOMO of the fluorophore, an electron transfers from the HOMO of the receptor to the HOMO of the fluorophore by the action of PeT, "locking" an electron in the LUMO and quenching the fluorescence. 70 Alternatively, when the receptor binds to a target, the energy level of the receptor HOMO is lowered below that of the



Scheme 14 The mechanism of PeT-based fluorescent probes.



Scheme 15 Frontier orbital explanation for the PeT effect.



Scheme 16 The recognition mechanism of probe NI-OPD towards

HOMO of the fluorophore. As such, the PeT process is blocked, and the fluorescence is restored (Scheme 15).

In 2018, Peng et al. reported a PeT-based endoplasmic reticulum (ER) targeting TP fluorescent probe NI-OPD, for detecting methylglyoxal (MGO),71 which is associated with diabetes and related complications (Scheme 16).72 NI-OPD contains a 1,8-naphthalimide fluorophore, and o-phenylenediamine (OPD) as the MGO recognition unit, with an additional methyl sulfonamide unit as an ER-targeting group. NI-OPD was non-fluorescent in PBS buffer (10% DMF, pH = 7.4) due to an "enhanced PeT" process from the OPD unit to the 1,8-naphthalimide moiety. Upon the addition of MGO, the dicarbonyl group of MGO reacted with the OPD group to form a stable adduct that inhibits PeT and affords a turn-on fluorescence (75fold) at $\lambda_{\rm em}=460$ nm ($\lambda_{\rm ex}=380$ nm). In addition, NI-OPD displayed excellent selectivity toward MGO over other aldehydes, including formaldehyde, acetaldehyde, benzaldehyde, glutaraldehyde, glyoxylic acid and o-phthalaldehyde (OPA). Furthermore, NI-OPD was evaluated in normal, diabetic and metformin treated diabetic mice to evaluate the difference in their endogenous MGO concentrations. The research indicated that NI-OPD could serve as a useful tool for evaluating the involvement of MGO in ER-associated diseases.

Nitric oxide (NO) is a ubiquitous biological messenger, and plays an active role in the regulation of various physiological processes in many biological systems, such as the cardiovascular, immune, and the central and peripheral nervous systems.73,74 In 2016, Guo et al. developed two fluorescent PeT based NO probes 4 and 5, where an N-benzyl-4-hydroxyaniline group was attached to a BODIPY fluorophore and used as the NO recognition group (Scheme 17).75 Probe 4 exhibited almost no fluorescence in PBS buffer (20% MeCN, pH 7.4) due to PeT from the N-benzyl-4-hydroxyaniline group to the excited BOD-IPY dye. However, under aerobic conditions, upon addition of NO, PeT was inhibited affording a dramatic fluorescence enhancement (92-fold) at $\lambda_{em}=518$ nm ($\lambda_{ex}=490$ nm). The introduction of a triphenylphosphonium (TPP) group within probe 4 afforded the mitochondrial targeting probe 5, which could specifically accumulate in the mitochondria of HeLa cells and was used to image exogenous NO. Guo and co-workers have also developed a similar probe 6 (Scheme 17),76 which exhibited a selective fluorescence off-on response towards NO and ONOO using N-benzyl-4-methoxyaniline as the reaction site

Perspective **Chemical Science**

Scheme 17 The structures of fluorescent probes 4, 5, 6, and 7.

rather than the N-benzyl-4-hydroxyaniline group. The results indicated that probe 6 exhibits a lower LoD (as low as 0.4 nM) and higher selectivity for NO than probe 4. Moreover, probe 6 could react with ONOO to produce an o-benzoquinone imine and induced significant fluorescence enhancement. Probe 6 displayed a significant fluorescence off-on response for both NO and ONOO in HeLa cells. Furthermore, mitochondriatargetable derivative probe 7 was developed by attaching a triphenylphosphonium group to probe 6, and was used to detect NO and ONOO in the mitochondria of HeLa cells.

Hydrogen peroxide (H₂O₂) plays an important role in cell growth, proliferation, host defence, immune response, and signalling pathways under physiological conditions.⁷⁷ In 2017, Kumar et al. reported a lysosome targeting PeT-based fluorescence probe LyNC for the detection of endogenous H2O2 in C6 and BV-2 cellular systems.78 LyNC was constructed using a catechol unit as response site for H₂O₂ and a morpholine moiety as a lysosome targeting group (Scheme 18). LyNC exhibited weak fluorescence in aqueous buffer (0.5% DMSO/ PBS, pH 7.4), due to the PeT effect from the catechol to the naphthalimide fluorophore. However, in the presence of H₂O₂, the catechol was oxidised to an o-quinone, which inhibited PeT thereby facilitating a fluorescence enhancement at λ_{em} = 537 nm ($\lambda_{ex} = 450$ nm). Furthermore, LyNC exhibited high

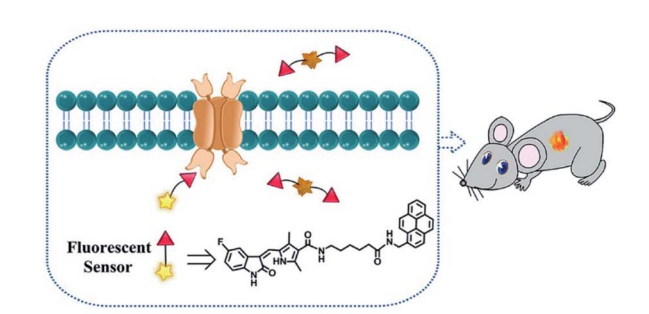
LVNC

Scheme 18 The recognition mechanism of probe LyNC towards H_2O_2 .

sensitivity toward H₂O₂ with a LoD of 0.22 μM, and excellent selectivity over other ROS/RNS and biothiols including cysteine, glutathione and homocysteine. Importantly, LyNC has been successfully used to detect H2O2 and in rat brain tissues and in living nematodes.

Duan et al. have developed a receptor-targeted fluorescent "off-on" probe SP1 for the detection and imaging of receptor protein-tyrosine kinases in vivo and in vitro.79 SP1 was composed of a sunitinib targeting group, a six-carbon bis(amide) linker and a pyrene fluorophore. The authors propose that the fluorescence of SP1 is quenched by dimer formation and π - π stacking interactions forming between the pyrene units and the fluorescence can be restored by binding of the sunitinib group with receptor protein-tyrosine kinases (Fig. 2). Initially, **SP1** displayed weak emission at $\lambda_{em} = 545$ nm ($\lambda_{ex} =$ 460 nm) in a DMSO/H₂O simulated physiological medium. In the presence of the protein-tyrosine kinase receptor, an "offon" fluorescence change was observed. SP1 was highly selective towards protein-tyrosine kinase receptor over other amino acids, inorganic salts, and other relevant substances. More importantly, SP1 was used to image tyrosine kinase in chick embryo chorioallantoic membrane and a HT-29 tumour-bearing mouse model, indicating that it could be used for real-time visualisation of tyrosine kinases in tumours.

By using PeT-based fluorescent probes, the localization, distribution and conformational changes of target molecules can be easily unveiled. When compared to sensors without fluorescence switches, PeT-based probes can easily achieve high signal-to-noise ratios, which is an essential requirement for satisfactory in vitro and in vivo fluorescence imaging. In addition, fluorescent prodrugs based on PET mechanisms are



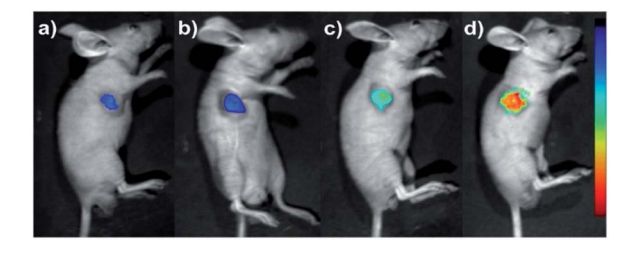
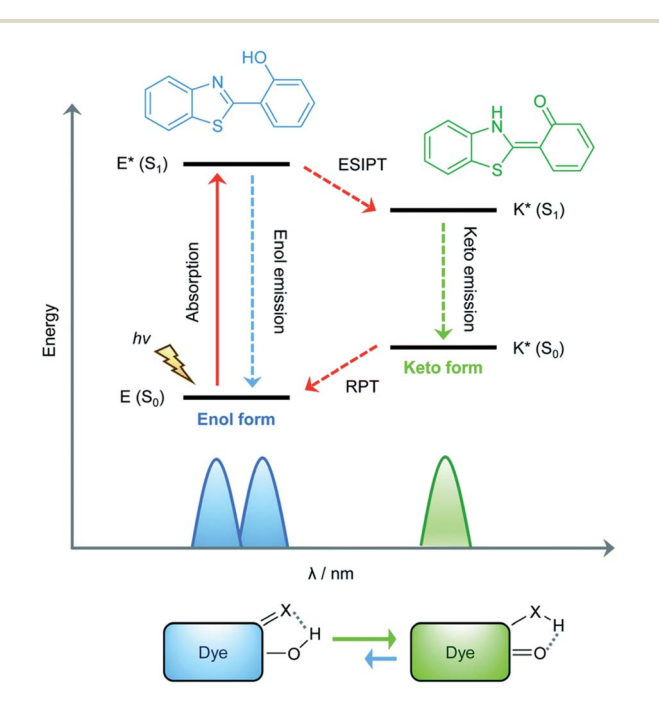


Fig. 2 Schematic diagram of SP1 and in vivo fluorescence imaging of SP1 in a HT-29 tumour-bearing mouse model via SP1 injection: (a) $0.1 \, \text{mM}$, $100 \, \mu \text{L}$; (b) $0.5 \, \text{mM}$, $100 \, \mu \text{L}$; (c) $1 \, \text{mM}$, $100 \, \mu \text{L}$; (d) $2 \, \text{mM}$, $100 \, \mu \text{L}$. The fluorescence signal was imaged at 500 to 720 nm under excitation with a 460 nm CW laser (power density of 1 mW cm⁻²). Reproduced with permission from ref. 79. Copyright 2018 American Chemical Society.

suitable agents for cancer diagnosis and therapy. So As such, the precise regulation of PeT processes is an avenue of development for the future improvement of PeT based prodrugs, which could improve the therapeutic effects and reduce the side effects in cancer treatment. However, a common disadvantage of PeT-based probes is the interference of protons, which also bind with the coordination site, inhibiting the PeT process, and enhancing the fluorescence. While, the development of PeT probes with lower pK_a values can offer a promising pathway for eliminating such proton interference.

5. Excited state intramolecular proton transfer (ESIPT) probes

The excited state intramolecular proton transfer (ESIPT) process was first reported by Weller in the 1950s.82 In general, ESIPT refers to the transfer of hydrogen atoms (mainly from hydroxyl or amino groups) to nearby heteroatoms (mainly N, O or S) under excitation.83 Fluorophores with ESIPT properties can establish a fast four-level photocycle between keto and enol isomers under excitation.13 ESIPT fluorophores, in the electronic ground state, usually exist in the enol (E) form. Upon photoexcitation, the electronic charge of the molecule is redistributed, leading to greater acidity of the hydrogen bond donor group and increased basicity of the hydrogen bond acceptor within the E form. Therefore, an extremely fast enol to keto phototautomerization $(K_{ESIPT} > 10^{12} \text{ s}^{-1})$ occurs: the excited state enol (E*) is rapidly converted to the excited ketone (K*). After a radiative decay pathway to the electronic ground state, a reverse proton transfer (RPT) takes place to produce the original E form (Scheme 19). The remarkable characteristics of



Scheme 19 Diagrammatic description of the ESIPT process. Reproduced with permission from ref. 13. Copyright 2018, The Royal Society of Chemistry.

Scheme 20 The structures of fluorescent probes NP1, NP2, NP3 and NP4

ESIPT fluorophores are: large Stokes shift,⁸⁴ and dual emission,^{85,86} which make them attractive units for the construction of functional fluorescent probes.

Li et al. have developed a series of 2-(2-hydroxyphenyl) benzothiazole-based (HBT-based) ESIPT probes NP1, NP2, NP3 and NP4 for the detection of ONOO with good specificity, fast response time, and high sensitivity (Scheme 20).87 NP1 responds rapidly to ONOO producing fluorescence enhancements in PBS (pH 7.4), however, it was found to be unstable when exposed to air, therefore, in order to improve molecular stability, NP2, NP3 and NP4 were developed. The hydroxyl group of HBT was switched to a N-methyl-p-hydroxyaniline, which blocked the hydrogen donor of the ESIPT process, and electrondonating groups (-OCH₃) were added to the p-hydroxyaniline ring in order to make the hydroxyl group more susceptible to oxidation. Exposure of NP3 to ONOO- results in the phenol group oxidizing to a benzoquinone imine, accompanied by N-C(sp²) bond cleavage, leading to a significant increase in the fluorescence intensity (600-fold). Moreover, NP3 was capable of crossing the blood-brain barrier (BBB) and could be used for TP fluorescence spectroscopy. The maximal TP absorption cross section of probe NP3 was determined to be 3.6 GM at 820 nm. This enabled probe NP3 to be used to visualize ONOO in neurovascular ischemia progression in the brains of live mice. The excellent properties of NP3 indicate that it could be used for visualizing other pathophysiological processes associated with ONOO-.

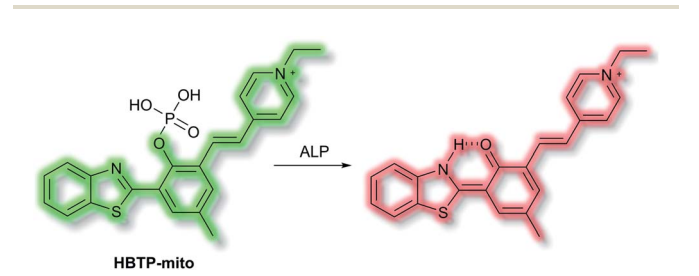
James and co-workers have developed an ESIPT-based ratiometric fluorescent probe **ABAH-LW** that facilitates the detection of ONOO $^-$ (Scheme 21). ** **ABAH-LW** was able to detect ONOO $^-$ within seconds and exhibits good selectivity and sensitivity towards ONOO $^-$ over other ROS and biologically relevant analytes. Initially, the benzyl boronic ester "protecting" unit of **ABAH-LW** blocks the ESIPT process. On exposure of **ABAH-LW** to ONOO $^-$, oxidative deprotection of the benzyl boronic ester unit occurs and leads to a ratiometric fluorescence response (I_{481nm}/I_{405nm}) with significant fluorescence enhancement (103-fold) in PBS buffer (8% DMSO, 1 mM CTAB, pH 8.2). Furthermore, the reactive chloroacetamide functional group of

Perspective Chemical Science

Scheme 21 The structures of fluorescent probes ABAH-LW and TCBT-OMe.

ABAH-LW enables covalent attachment to biomacromolecules located at the ER enabling the visualization of ONOO within the ER. ABAH-LW was shown to be cell permeable, which enabled it to be used to visualize ONOO in live HeLa cells. The same group also developed a HBT-based fluorescent probe TCBT-OMe for the detection of HOCl/ClO⁻ (Scheme 21).89 The presence of HClO/ClO- leads to the hydrolysis of the dimethylthiocarbamate moiety resulting in a large increase in fluorescence intensity (~42 fold) at $\lambda_{em}=472$ nm ($\lambda_{ex}=310$ nm). Probe TCBT-OMe was shown to have high sensitivity (LoD = 0.16 nM) and selectivity towards HClO/ClO over other ROS/ RNS and can be used to detect endogenous and exogenous HClO/ClO in HeLa cells. In addition, test strips containing TCBT-OMe were constructed and could be used to detect HClO/ ClO in drinking water. Furthermore, TCBT-OMe was used as dual input logic gate for Hg2+ and H2O2. Interestingly, the addition of Hg2+ alone to TCBT-OMe resulted in a significant increase in the fluorescence intensity (within 30 min), which is believed to due to the instability of the dimethylcarbamate (incorrectly written as dimethylcarbonate in the original paper) formed from the reaction of **TCBT-OMe** with Hg^{2+} .

Zhang *et al.* have developed a novel mitochondria-targeted HBT-based ESIPT fluorescent probe **HBTP-mito** that facilitates the detection of ALP.⁹⁰ **HBTP-mito** is comprised of the HBT fluorophore and the pyridinium salt as a mitochondrial targeting group (Scheme 22). Initially, the ESIPT process of the phosphorylated probe is blocked and it exhibits fluorescence at $\lambda_{\rm em} = 514$ nm. However, in the presence of ALP, hydrolysis of



Scheme 22 The structures of fluorescent probe HBTP-mito.

the phosphate ester and cleavage of the P–O bond releases HBT resulting in ESIPT turn on, and the emission switches from green ($\lambda_{\rm em}=514$ nm) to red ($\lambda_{\rm em}=650$ nm, Scheme 22) in TBS buffer solution (pH 8.0). Probe **HBTP-mito** exhibited high sensitivity (LoD = 0.072 mU mL $^{-1}$) and excellent selectivity for ALP over other anions, and ions. In addition, the $I_{514\text{nm}}/I_{650\text{nm}}$ ratiometric response of the enzymatic hydrolysis product prevented fluorescence interference from the serum. Therefore, it could be used for detecting ALP in serum samples. Due to the low toxicity of **HBTP-mito**, it was suitable for monitoring ALP activity *in vitro* and *in vivo* and provided a blue-print for constructing ratiometric probes with longer wavelength emission and high sensitivity.

Recently, Feng and co-workers have developed a fluorescent probe CORM3-green based on an ESIPT phthalimide dye for the detection of CORM-3 in both solution and living systems.91 CO-Releasing molecules (CORMs) are agents that release and deliver CO into the cell and can be used to replace the direct use of CO gas in the treatment of diseases.92 CORM3-green is nonfluorescent, however, upon addition of CORM-3, the nitro group is reduced into an amino group to form a highly fluorescent phthalimide, which emits bright green fluorescence at $\lambda_{\rm em} = 503$ nm in PBS buffer (0.5% DMSO, pH 7.4) solution due to the ESIPT process (Scheme 23). Furthermore, CORM3-green exhibited high sensitivity toward CORM-3 with a LoD of 16 nM, and excellent selectivity over other anions, metal ions, amino acids, ROS/RNS and biothiols including cysteine, glutathione and homocysteine. CORM3-green was evaluated in solution and in HeLa cells, zebrafish, and mice, thus demonstrating its use as a potentially powerful visualizing agent for biological applications.

James *et al.* have reported a series of 3-hydroxyflavone (3-HF) ESIPT boronate-based fluorescent probes that exhibit a ratiometric response toward ONOO⁻ in micellar environments

Scheme 23 The structures of fluorescent probes CORM3-green.

Scheme 24 ESIPT probes 3-HF-X (X = OMe, Me, H) for detecting ONOO $^-$. The normal (N) and phototautomeric (T*) forms are shown.

Chemical Science Perspective

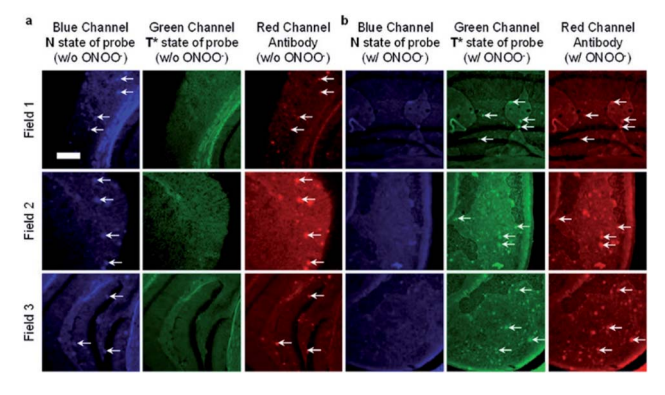


Fig. 3 Fluorescence imaging of a brain section of a transgenic mouse treated with 3-HF-OMe (20 μ M) (a) without and (b) with ONOO⁻ (30 μ M). The excitation/emission wavelengths for the blue (N-state), green (T*-state), and red (anti-A β antibody) channels are 404/425–475, 404/500–550, and 561/640–730 nm, respectively. The white arrows indicate stained A β aggregates. Reprinted from ref. 93. Copyright 2018, American Chemical Society.

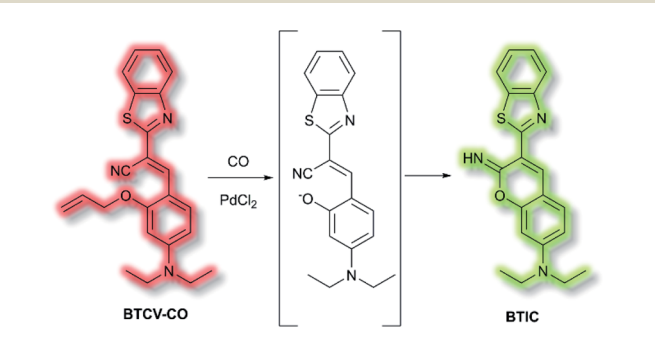
(Scheme 24).93 Probe 3-HF-OMe, is particularly sensitive toward hydrophobic environments and is able to differentiate between micellar and aqueous environments. The benzyl boronic ester "protecting" group blocks the ESIPT process, and the group can be selectively removed by ONOO⁻. Therefore, probe 3-HF-OMe was found to produce a ratiometric fluorescence response when bound to Aβ aggregates (hydrophobic environment) in the presence of ONOO-. To investigate the potential of the probe for real world applications, fluorescence imaging of 3-HF-OMe exhibited N-state fluorescence in mice brain slices (Fig. 3, blue channel) associated with AB aggregates as shown by correlation with anti-Aβ42 antibodies (Fig. 3, red channel). Then addition of ONOO to the brain sections, generated the T* state of 3-HF-OMe (Fig. 3, green channel), which correlated well with the antibody fluorescence. As such these preliminary biological imaging experiments indicate how similar but longer wavelength ESIPT-based probes could be used to monitor fibrous proteins/peptides and environmental ROS/RNS. This system was described by the authors as a "reactive species" and "environment" based fluorescent probe.

Due to the unique transient nature of the four-level photochemical process of ESIPT, the ESIPT emission is highly sensitive to its local surroundings. Moreover, ESIPT fluorophores exhibit unusually large Stokes shifts (\sim 200 nm), when compared to traditional fluorophores (fluorescein, rhodamine, *etc.*). This helps avoid unwanted self-reabsorption and inner-filter effects. The limitation of ESIPT-based fluorescent probes come from the presence of polar and hydrogen bond donor solvents, which can lead to inhibition of the ESIPT process with no ketone (K*) emission. However, their use in combination with other fluorescence mechanisms will allow the construction of new probes that overcome the limitations of many current detection methods, while allowing the development of more and more practical fluorescence-based sensors and imaging agents. ⁹³

6. Aggregation induced emission (AIE) probes

Ordinarily, aggregation of fluorescent probe molecules is considered detrimental, resulting in aggregate-caused quenching (ACQ). The ACQ process is often exacerbated when a probe has multiple conjugated aromatic rings due to the increased formation of exciplexes and excimers.94 However, in 2001 the Tang group reported that 1-methyl-1,2,3,4,5-pentaphenylsilole exhibited the opposite effect - upon aggregate formation, a significant enhancement in photoluminescence was observed.95 The emission was ascribed to the severe steric hindrance of the fluorophore - since upon aggregation, the compound was unable to adopt a uniformly planar conformation. The process was termed 'aggregation-induced emission', and since then the area has expanded exponentially. Further investigations have elucidated that one common mechanism of AIE is the restriction of intramolecular motion (RIM).96 Such probes show negligible fluorescence in solution and exhibit a significant 'turn-on' upon aggregation. Common application of AIE compounds include use in electroluminescent devices and use as fluorescent sensors and dosimeters. 97 In particular, AIE has been used in the field of biological fluorescence, for example in cell imaging, tumour imaging, and enzyme detection.98 Such probes are often referred to as 'AIEgens'. The Tang group have published comprehensive reviews on, and extensive descriptions of, the AIE phenomenon, in particular their 2015 article 'Aggregation-Induced Emission: Together We Shine, United We Soar'.14

In 2019, Tang *et al.* published an AIE probe for imaging carbon monoxide (CO). ⁹⁹ Whilst known for its toxicity, CO is also an endogenous gasotransmitter and is involved in a range of disease states and biological pathways. The probe, **BTCV-CO**, was designed to undergo a Tsuji–Trost reaction in the presence of CO and Pd²⁺ (Scheme 25). In solution, **BTCV-CO** was found to fluoresce at $\lambda_{\rm em} \approx 675$ nm. Solution aggregation experiments with the probe confirmed the AIE characteristics. Mechanistically, it has been proposed that in solution rapid non-radiative decay can occur from the singlet excited state, mediated by *cistrans* isomerisation of the trisubstituted alkene. Then, upon aggregation the isomerisation pathway is hindered. Therefore, formation of **BTIC** *via* the Tsuji–Trost reaction would similarly prevent this *cis–trans* isomerisation. Studies in PBS (5% DMSO,



Scheme 25 Detection of CO by AlEgen BTCV-CO.

v/v, pH 7.4) with CO donor [Ru(CO)₃Cl₂]₂ (CORM-2) and PdCl₂ confirmed the expected fluorescent enhancement. On formation of BTIC, a new emission band at $\lambda_{\rm em} = 546$ nm was observed, facilitating the ratiometric $\left(I_{546\mathrm{nm}}/I_{710\mathrm{nm}}\right)$ detection of CO. The ratiometric response of BTCV-CO to CO was more sensitive than just the turn-on response, affording fluorescent enhancements of 39-fold and 17-fold respectively. The ratiometric enhancement was found to correlate with increasing concentrations of CORM-2, which scaled linearly at low concentrations (1-5 µM). Furthermore, the probe was found to be selective towards CO over a range of biological analytes (including ROS, RNS, amino acids, and common anions), and the detection limit of BTCV-CO towards CO was determined to be 30.8 nM. Exogenous addition of CO (via CORM-2) to cells loaded with BTCV-CO confirmed that the cells underwent fluorescent enhancement in the green window ($\lambda_{ex} = 476$ nm, $\lambda_{\rm em} = 500\text{--}580 \text{ nm}$) relative to cells loaded with only the probe which showed weak emission in both the green and red (λ_{em} = 580-700 nm) windows. Enhancement of the ratiometric response was found to correlate with the concentration of CO added. Furthermore, in vivo evaluation confirmed that a significant fluorescent response could be achieved in mice injected with BTCV-CO + CORM-2 + PdCl₂, whereas injection with only BTCV-CO + PdCl₂ resulted in only weak emission.

An extensive area of the NIR AIE literature concerns probes for tumour sensing and imaging, particularly as contrast agents. ^{100,101} In 2015, Zhu *et al.* designed a series of tumourtargeting probes based on quinoline–malononitrile AIE fluorophores conjugated to a range of electron-donating motifs *via* thiophene linkers (Fig. 4). ¹⁰² Probes **QM-3** to **QM-6** were found to exhibit NIR AIE behaviour in solution. Notably, increasing the electron-donating character of the triphenylamine moiety in

Fig. 4 Structures of AlEgens QM-3-QM-6.

QM-3, QM-5, and QM-6 resulted in a redshift of the AIE. A 3,4ethylene-dioxythiophene (EDOT) moiety was introduced to compounds QM-4, QM-5, and QM-6 to tailor the AIE by altering the donor- π -acceptor system through the resultant change in conformation. This resulted in increased aggregation control with the solution-based studies. Imaging of evaporation experiments, to simulate aggregation, revealed that QM-3 adopted a microrod structure whilst QM-4-QM-6 formed spherical nanoparticles. The difference in morphology was attributed to the introduction of the EDOT moiety in the latter species. Furthermore, the photostability of each species was found to be ≈ 20-fold greater than commercially available dye ICG. QM-5 exhibited the most desirable characteristics and was evaluated in cells. The probe underwent rapid uptake and spherical aggregate formation in HeLa cells. Furthermore, QM-5 remained fluorescent 24 h after incubation and was emissive for twice as many cell passages as the ICG control. In vivo experiments in mice indicated that QM-5 was tumour specific, affording an AIE response within 30 minutes. Furthermore, the probe was tumour retentive, remaining in tumour tissue for 24 h. The tumour specificity was ascribed to the enhanced permeability and retention (EPR) effect afforded by the spherical shaped aggregates. Ex vivo organ imaging of injected mice indicated that whilst QM-5 aggregated in tumour tissue, it also aggregated in the liver.

In 2020, Wu *et al.* designed an NIR probe for the detection of breast cancer metastasis, combining AIE and multispectral optoacoustic tomography (MSOT). The group used a donor- π -acceptor system of dihydroxanthene and quinolinium groups respectively, using a nitroaryl recognition moiety to afford **Q-NO**₂. Upon reduction of the nitro group by nitroreductase, the resultant amine undergoes self-immolation of the *p*-benzyl moiety to afford phenol **Q-OH** (Scheme 26). Fluorescent enhancement occurred at $\lambda_{\rm em}=780$ and 922 nm when excited at $\lambda_{\rm ex}=680$ and 808 nm respectively due to the formation of **Q-OH** aggregates; the fluorescence intensity at each emission

Scheme 26 Nitroreductase detection mechanism by AlEgen Q-NO₂.

Chemical Science Perspective

band was found to increase linearly with increasing concentrations of nitroreductase. Furthermore, a linear optoacoustic response with increasing nitroreductase was observed. The probe was found to be highly selective over a range of relevant biological analytes, and a detection limit of 0.052 μg mL⁻¹ towards nitroreductase was established. For cell testing, 4T1 murine mammary carcinoma cells were chosen due to their overexpression of nitroreductase. Hypoxic cells, known to overexpress nitroreductase, stained with Q-NO2 displayed a turn on-response for both the NIR-I and NIR-II window, compared to control cells which exhibited minimal fluorescence. In addition, an optoacoustic response that mirrored that of the fluorescence response was observed. Q-NO2 was shown to detect orthotopic and far metastatic tumours in the mouse models used, with an enhanced NIR-I and NIR-II response relative to the bioluminescence control. Tumour imaging via the NIR-II window afforded a clearer image of the tumours due to the decreased autofluorescence. Notably, MSOT imaging of mice with Q-NO₂ was able to effectively monitor both orthotopic tumour growth and eventual metastasis in 3D.

Aβ is another key biological target, due to its role in the pathogenesis of Alzheimer's disease. In 2019, Zhu et al. described a new NIR AIE probe for the imaging of Aβ plaques.¹⁰⁴ The authors sought to design a probe that improved on commercial probe Thioflavin T (ThT), which suffers from ACQ, low signal-to-noise ratio, and low BBB penetration. Probe QM-FN-SO₃ incorporated the quinoline-malononitrile NIR fluorophore, to which a conjugated thiophene was attached to increase lipophilicity and aid BBB penetration. In addition, a sulfonate group was added to increase water solubility and generate a 'fluorescence-off' state when not aggregated (Fig. 5). Probe QM-FN-SO3 was non-fluorescent in water but a turn-on fluorescence response ($\lambda_{ex} = 500\,$ nm, $\lambda_{em} = 720\,$ nm) was observed as the solubility of the probe decreased and aggregation began. In PBS solution, QM-FN-SO3 displayed a positive AIE response to Aß aggregates, for which fluorescent enhancement (blue-shifted to $\lambda_{em} = 665$ nm) increased as the concentration of Aβ aggregates increased. Mechanistically, it was proposed that the N-dimethylamino group acts as a recognition moiety, which once bound experiences reduced freedom of rotation, affording a fluorescence response. The half-life of QM-FN-SO3 was found to be $\approx 5 \times$ that of ThT at ≈ 40 min and exhibited a greater signal-to-noise ratio both in solution and in mouse brain models evaluated. Furthermore, in vivo evaluation using mouse models indicated that could QM-FN-SO3 cross the BBB and

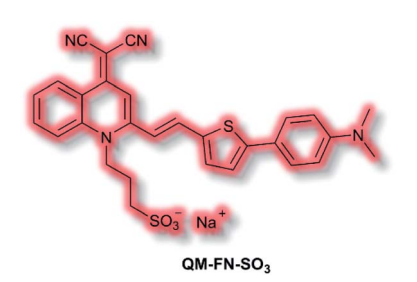


Fig. 5 Structure of AlEgen QM-FN-SO₃

produce a fluorescence response to $A\beta$ plaques in the hippocampus.

An obvious advantage for the AIE strategy is the ability to overcome the quenching issues presented by ACQ. Furthermore, for turn-on AIEgens, the probe is non-fluorescent in solution. As a fluorescent signal is only observed upon aggregation, as such there is no overlap between the signal of the species involved in the sensing process, and the process is independent of the probe concentration. Due to the size of their extensive π -systems, some AIEgens can suffer from increased hydrophobicity, which may lead to issues with cellular uptake and distribution.

7. Multiple modality fluorescent probes

Fluorescent chemosensors have been widely applied in diverse fields such as biology, physiology, medicine, and pharmacology. Fluorescence output signals can be observed using optical instruments and even using the naked eye in real-time. ¹⁶ Fluorescent chemosensors generally exhibit changes in fluorescence intensities and wavelength using various single sensing mechanisms, including ICT, PeT, FRET, ESIPT and AIE. ^{12,50,106,107} However, fluorescent chemosensors can also be designed based on dual (or multiple) fluorescence mechanisms in order to deliver diverse fluorescence outputs, facilitating the simultaneous tracking of multiple analytes or improving the selectivity and sensitivity for a particular analyte.

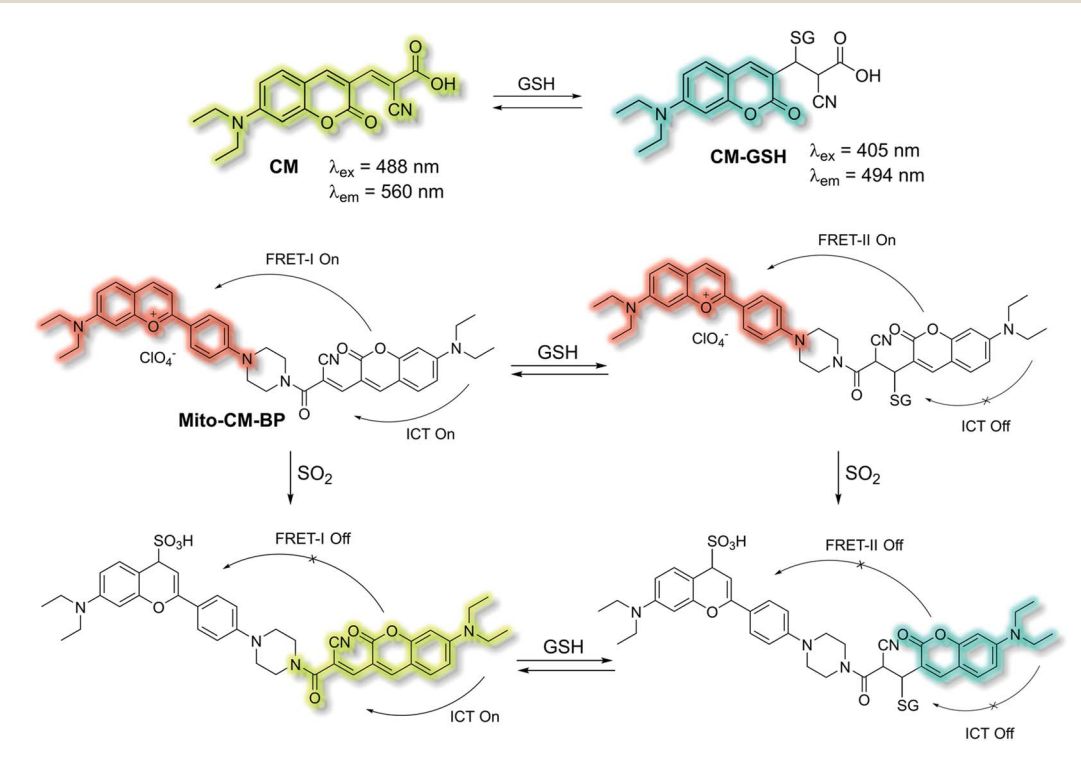
 H_2S and hydrogen polysulfides $(H_2S_n, n > 1)$ are endogenous regulators of many physiological processes,108 and data suggest that H_2S_n might be the main signalling molecules instead of H₂S. In order to reveal the mutual relationship and cellular cross-talk between H_2S and H_2S_n in cells, Xian et al. reported a dual-channel fluorescent probe DDP-1 using a rhodolcoumarin hybrid for visualizing H_2S and H_2S_n using different fluorescence signals.109 With DDP-1, an azidocoumarin moiety and phenyl 2-(benzoylthio)benzoate were chosen as the reaction sites for H₂S and H₂S_n. When H₂S_n reacts with the phenyl-2-(benzoylthio)benzoate, the green fluorescence of rhodol at λ_{em} = 542 nm ($\lambda_{\rm ex}$ = 360 nm) was observed (Scheme 27). However, on the addition of H₂S, the situation is more complicated since the reaction between H2S and azides led to the formation of H_2S_n , however, less than 0.5 equivalents of H_2S_n are produced from the reaction of H2S (1 equivalent) and azide, which means the reaction with H2S produced both the blue coumarin emission at $\lambda_{em} = 445$ nm (major) and green rhodol emission at λ_{em} = 542 nm (minor) (λ_{ex} = 360 nm). Therefore, **DDP-1** can detect H_2S and H_2S_n using these two distinct emission channels. As such DDP-1 could be used for the detection of H₂S and H₂S_n in HeLa cells.

Yin et al. have developed a novel dual-functional fluorescent probe Mito-CM-BP based on an ICT-FRET mechanism for the simultaneous detection of GSH and SO₂ (Scheme 28).¹¹⁰ The probe consists of an ICT based coumarin-cyanoacetic acid system as an energy donor and a reaction site for GSH; while the benzopyrylium unit (BP) can not only serve as an energy

DDP-1 detection of H₂S and H₂S_n using two distinct emission channels.

acceptor but also as a sensitive reaction site for SO2. Two excitation wavelengths at $\lambda_{ex} = 488$ and $\lambda_{ex} = 405$ nm, which correspond to CM (donor of FRET-I) and CM-GSH (donor of FRET-II), were chosen as there are two different FRET systems before and after Mito-CM-BP reacts with GSH. The free probe Mito-CM-BP displayed a fluorescence emission at $\lambda_{em} = 638 \text{ nm}$ ($\lambda_{\rm ex} = 488$ nm). Then upon addition of SO₂, the FRET-I process of Mito-CM-BP was blocked, and the fluorescence emission at

638 nm gradually decreased and a shorter wavelength emission at 560 nm appeared. Conversely, exposure of Mito-CM-BP to GSH resulted in destruction of the π -conjugation between coumarin and cyanoacetic acid. The inhibition of the ICT process triggers a FRET-II process from the CM-GSH donor to the BP acceptor, leading to a significant fluorescence enhancement at $\lambda_{ex} = 638$ nm ($\lambda_{ex} = 405$ nm). Furthermore, addition of SO2 breaks the conjugated system of the BP moiety,



Scheme 28 ICT and FRET-based probe Mito-CM-BP developed to allow for the simultaneous detection of GSH and SO₂.

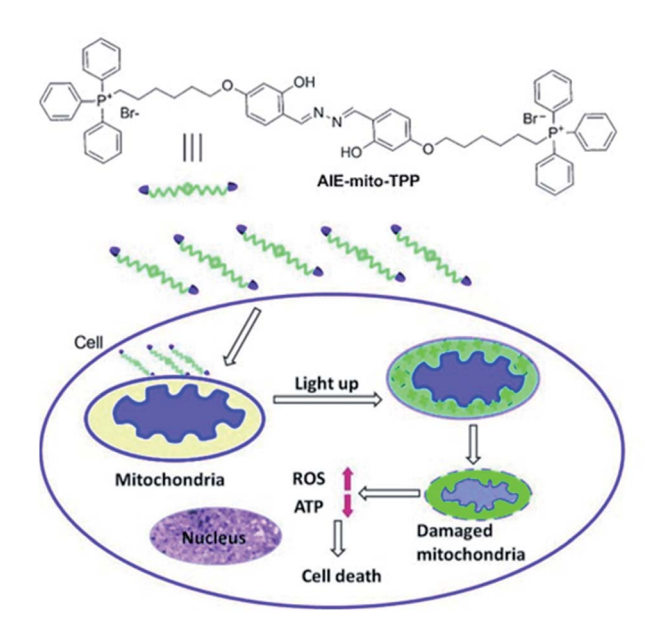
which stops the FRET-II process, resulting in an increase in emission at $\lambda_{\rm em}=494$ nm and decrease in emission at $\lambda_{\rm em}=638$ nm. Importantly, **Mito-CM-BP** has been successfully used for the visualization of enzymatic conversion of intracellular GSH to SO_2 in different cell lines (HepG2 and SW480 cells) and tumour-bearing mice, which may help to clarify the metabolic pathways of SO_2 production and facilitate an understanding of the role of SO_2 in biological systems.

Chemical Science

In 2018, Dhara et al. developed a lysosome targeting CO fluorescent probe LysoFP-NO2, consisting of a naphthalimide fluorophore, a nitro group as the CO responsive moiety, and a morpholine fragment as the lysosome-targeting unit (Scheme 29).111 LysoFP-NO2 displayed weak fluorescence due to the strong electron withdrawing ability of the nitro group, which can guench the fluorescence of the fluorophores by PeT. However, upon the addition of CO, the nitro group was converted into an amino moiety, stopping PeT and strengthening the ICT process. Therefore, probe LysoFP-NO₂ displayed a "turn on" fluorescence response towards CO with a 75-fold fluorescence enhancement in HEPES buffer (1% DMSO, pH 7.4). In addition, probe LysoFP-NO2 displayed high selectivity over other relevant reactive nitrogen, oxygen, and sulfur species. Moreover, LysoFP-NO2 could be used to monitor changes in intracellular CO within the lysosomes of live MCF7 cells.

Liu et al. have developed a mitochondria-targeting probe AIE-mito-TPP based on an AIE and ESIPT system as an imaging agent and potential chemotherapeutic drug.112 Triphenylphosphonium (TPP), a positively charged lipophilic cation, is a wellknown mitochondrial targeting ligand due to the negative potential gradient of the organelle.113 AIE-mito-TPP consists of a salicylaldazine fluorophore attached to two TPP groups for targeting the mitochondria (Scheme 30). The salicylaldazine fluorophore uses two emission mechanisms: AIE via restriction of intramolecular rotation around the N-N bond and ESIPT caused by intramolecular hydrogen bonds. AIE-mito-TPP was almost non-fluorescent in cell-culture media but the fluorescence due to both AIE and ESIPT is activated in mitochondria ($\lambda_{ex} = 543$ nm, $\lambda_{em} = 575\text{-}625$ nm). Furthermore, AIE-mito-TPP accumulated preferably in cancer cell mitochondria and exhibited selective cytotoxicity towards cancer cells which was attributed to the difference in mitochondrial membrane potential between normal and cancerous cells. In addition, AIEmito-TPP could induce mitochondrial dysfunction influencing

Scheme 29 $\,$ A lysosome targetable fluorescent probe $LysoFP\text{-}NO_2$ for detection of CO.



Scheme 30 The structure of probe AIE-mito-TPP and schematic representation of intracellular tracking and the therapeutic effect of AIE-mito-TPP in cancer cells. Reprinted from ref. 112. Copyright 2014, Wiley-VCH Verlag GmbH & Co. KGaA, Weinheim.

several important cellular processes and facilitating the selective killing of HeLa cells.

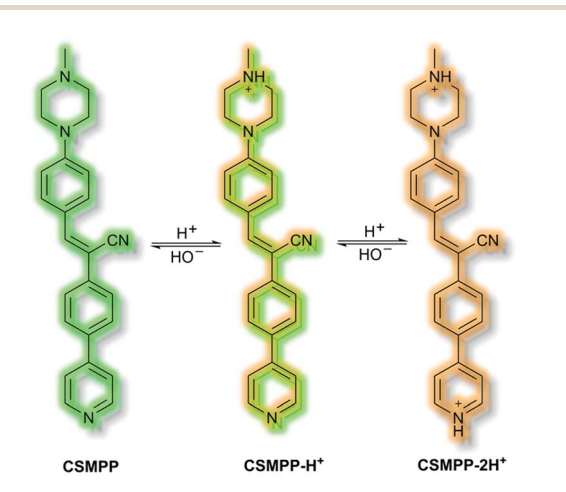
As discussed in the section on ICT probes, β -gal is a known biomarker for ovarian cancer. In 2019, Guo *et al.* reported a probe for monitoring β -gal activity, designed around the commonly used AIE quinoline–malononitrile fluorophore. ¹¹⁴ A 2-(2-hydroxyphenyl)benzothiazole moiety was conjugated to both increase lipophilicity and extend the π -system to favour NIR emission. A galactose residue was attached to the probe to act as the recognition moiety, to give the probe **QM-HBT-\betagal**. In PBS solution (30% DMSO, v/v, pH 7.4) **QM-HBT-\betagal** produced a turn on response at $\lambda_{\rm em} = 650$ nm ($\lambda_{\rm ex} = 460$ nm) in the presence of β -gal. It was proposed that the saccharide moiety of **QM-HBT-\betagal** increased the hydrophilicity of the

Scheme 31 Detection of β -gal by combined AIE-ESIPT probe QM-HBT- β gal.

Perspective Chemical Science

probe; and upon cleavage by β -gal, the resulting **QM-HBT-OH** was insoluble in solution and aggregated to give an AIE response (Scheme 31). Furthermore, cleavage of the sugar moiety unmasks the ESIPT system upon formation of the hydroxyl moiety. An increase in emission at 650 nm occurred, scaling linearly, with added β -gal. Furthermore, the probe was found to be highly selective (over other assayed enzymes and amino acids), was stable over a pH range from 3 to 11, and exhibited a 60-fold greater half-life than commercial standard ICG. Due it is excellent performance in solution, QM-HBT- β gal was then evaluated for the *in vivo* detection of β -gal. **QM-HBT-** β gal exhibited no fluorescence in HeLa cells without exogenous addition of β -gal, whereas SKOV-3 cells exhibited significant fluorescence enhancement with the probe due to high endogenous β -gal expression. Inhibition studies confirmed that the AIE response originated from β -gal activity.

Recently, in 2020 the Tang group proposed an AIE lysosome targeting probe for monitoring lysosomal pH during the tissue regeneration process.115 Lysosomes play a key role in tissue regeneration, for which pH 4-5 is essential for lysosomal hydrolase activity. Whilst research has been conducted on lysosomes and tissue regeneration, an in vivo study of lysosome pH during the regeneration process had not previously been reported. Probe CSMPP was designed around an α-cyanostilbene fluorophore, to which a piperazine moiety was attached to target the lysosome. In solution (MeCN), CSMPP was found to be weakly fluorescent at $\lambda_{em} = 509$ nm ($\lambda_{ex} = 365$ nm) but the fluorescence enhanced upon addition of water (MeCN/water, 2/ 8, v/v) due to aggregation. By varying the pH of CSMPP in solution, a ratiometric emission response was observed; relative to neutral solutions, at acidic pH the emission band at λ_{em} = 509 nm decreased and a new emission at $\lambda_{em} = 615$ nm increased. The process was found to be reversible. The acid sensitivity of the probe was ascribed to the piperazine and pyridine moieties (Scheme 32). Furthermore, DFT calculations indicated that protonation of the pyridine moiety afforded enhanced ICT, imparting a ratiometric response upon protonation. Staining of HeLa and ARPE-19 cells confirmed that CSMPP could selectively target lysosomes, with Pearson



Scheme 32 Combined AIE-ICT probe CSMPP.

coefficients of 0.92 and 0.90 respectively. *In vivo* NIR confocal studies with medaka larvae indicated that **CSMPP** was able to target lysosomes in the larval fin with good specificity. **CSMPP** was then used to study the regeneration process of injured medaka caudal fins *in vivo*. Relative to a control group which saw almost no lysosomal pH change, healing caudal fins were shown to undergo a range of pH changes post-amputation. Within 24 h, the pH dropped from 5.1 to 4.6 due to increased lysosomal activity. Interestingly, the pH of lysosomes adjacent to the injury were found to be more acidic than those further away. As the tissue regenerated, the pH returned to normal after 5 days.

Compared to single sensing mechanism-based sensors, dual/triple sensing mechanism-based sensors generally produce changes in the emission intensity and wavelength of the signals at the same time, which can provide different fluorescence signals or amplify the response signals.16 This is highly desirable for the simultaneous monitoring of multiple analytes or improving the selectivity and sensitivity of fluorescence sensors. Furthermore, the signal-to-noise ratio would significantly increase when the two/multiple mechanisms have similar effects on the same chromophore. We anticipate that dual and multi mechanism based fluorescent sensors will be employed for exciting applications in various fields, especially in high signal-to-noise ratio fluorescence bioimaging, investigating interactions among multiple biological species, and the development of optical logic devices with multiple inputs and outputs.

8. Conclusions

Over the last decade there have been considerable advances in the development of molecular fluorescent probes used for biological sensing and imaging, advancing our understanding and guiding our treatment of a diverse range of medical conditions. In particular, the development of high-resolution techniques including STORM, PALM and PAI etc. have invigorated the area by encouraging the de novo design of probes with improved photophysical properties and targeting ability. With this perspective we have highlighted some of the recent developments made in the design of such fluorescent probes, using the following approaches: FRET; ICT; PeT; ESIPT; AIE and probes combining these modalities. Each probe has been selected based on its ability (or potential), for detecting analytes of interest in a real-world environment. In addition, we have highlighted the advantages and disadvantages of each fluorescence based approach. We end with a section outlining how some disadvantages of individual fluorescence based systems can be overcome through the combination of multiple fluorescence techniques.

In summary, with this perspective we believe we have highlighted recent progress made in the development of fluorescent probes using singular and multiple modality fluorescence approaches. From this perspective, it is clear that the area of fluorescent probes used for biological applications will continue to be challenged and pushed forward by the development of enhanced measurement techniques, that require **Chemical Science**

improved photophysical properties and targeting ability, beyond what is currently available.

Conflicts of interest

There are no conflicts to declare.

Acknowledgements

XT wishes to thank the University of Bath for supporting her PhD work in the UK. LCM wishes to thank EPSRC for DTP PhD funding. LW wishes to thank China Scholarship Council and the University of Bath for supporting his PhD work in the UK. SEL wishes to thank EPSRC for funding (EP/R51164X/1). TDJ wishes to thank the Royal Society for a Wolfson Research Merit Award and the Open Research Fund of the School of Chemistry and Chemical Engineering, Henan Normal University for support (2020ZD01).

Notes and references

- 1 A. P. de Silva, H. Q. N. Gunaratne, T. Gunnlaugsson, A. J. M. Huxley, C. P. McCoy, J. T. Rademacher and T. E. Rice, Chem. Rev., 1997, 97, 1515-1566.
- 2 J. S. Kim and D. T. Quang, Chem. Rev., 2007, 107, 3780-3799.
- 3 X. Chen, T. Pradhan, F. Wang, J. S. Kim and J. Yoon, Chem. Rev., 2012, 112, 1910-1956.
- 4 D. Wu, A. C. Sedgwick, T. Gunnlaugsson, E. U. Akkaya, J. Yoon and T. D. James, Chem. Soc. Rev., 2017, 46, 7105-
- 5 J. Chan, S. C. Dodani and C. J. Chang, Nat. Chem., 2012, 4, 973-984.
- 6 H.-W. Liu, L. Chen, C. Xu, Z. Li, H. Zhang, X.-B. Zhang and W. Tan, Chem. Soc. Rev., 2018, 47, 7140-7180.
- 7 Y. Yue, F. Huo, F. Cheng, X. Zhu, T. Mafireyi, R. M. Strongin and C. Yin, Chem. Soc. Rev., 2019, 48, 4155-4177.
- 8 Y. Yue, F. Huo, F. Cheng, X. Zhu, T. Mafireyi, R. M. Strongin and C. Yin, Chem. Soc. Rev., 2019, 48, 4336-4337.
- 9 Y. Fu and N. S. Finney, RSC Adv., 2018, 8, 29051-29061.
- 10 H. Kobayashi, M. Ogawa, R. Alford, P. L. Choyke and Y. Urano, Chem. Rev., 2010, 110, 2620-2640.
- 11 L. Wu, C. Huang, B. P. Emery, A. C. Sedgwick, S. D. Bull, X.-P. He, H. Tian, J. Yoon, J. L. Sessler and T. D. James, Chem. Soc. Rev., 2020, 49, 5110-5139.
- 12 B. Daly, J. Ling and A. P. de Silva, Chem. Soc. Rev., 2015, 44, 4203-4211.
- 13 A. C. Sedgwick, L. Wu, H.-H. Han, S. D. Bull, X.-P. He, T. D. James, J. L. Sessler, B. Z. Tang, H. Tian and J. Yoon, Chem. Soc. Rev., 2018, 47, 8842-8880.
- 14 J. Mei, N. L. C. Leung, R. T. K. Kwok, J. W. Y. Lam and B. Z. Tang, Chem. Rev., 2015, 115, 11718-11940.
- 15 Z. Zhao, H. Zhang, J. W. Y. Lam and B. Z. Tang, Angew. Chem., Int. Ed., 2020, 59, 9888-9907.
- 16 L. He, B. Dong, Y. Liu and W. Lin, Chem. Soc. Rev., 2016, 45,
- 17 M. Bates, B. Huang, G. T. Dempsey and X. Zhuang, Science, 2007, 317, 1749-1753.

- 18 E. Betzig, G. H. Patterson, R. Sougrat, O. W. Lindwasser, S. Olenych, J. S. Bonifacino, M. W. Davidson, J. Lippincott-Schwartz and H. F. Hess, Science, 2006, 313, 1642-1645.
- 19 P. Beard, Interface Focus, 2011, 1, 602-631.
- 20 J. Xia, J. Yao and L. V. Wang, Prog. Electromagn. Res., 2014, **147.** 1-22.
- 21 J. Shi, Y. Tang and J. Yao, Quant. Imaging Med. Surg., 2018, 8, 724-732.
- 22 M. H. Lee, N. Park, C. Yi, J. H. Han, J. H. Hong, K. P. Kim, D. H. Kang, J. L. Sessler, C. Kang and J. S. Kim, J. Am. Chem. Soc., 2014, 136, 14136-14142.
- 23 J. Zhao, D. Zhong and S. Zhou, J. Mater. Chem. B, 2018, 6, 349-365.
- 24 J. Cao, B. Zhu, K. Zheng, S. He, L. Meng, J. Song and H. Yang, Front. Bioeng. Biotechnol., 2020, 7, 487.
- 25 M. Gao, F. Yu, C. Lv, J. Choo and L. Chen, Chem. Soc. Rev., 2017, 46, 2237-2271.
- 26 C. Li, G. Chen, Y. Zhang, F. Wu and Q. Wang, J. Am. Chem. Soc., 2020, 142, 14789-14804.
- 27 R. Weissleder, Nat. Biotechnol., 2001, 19, 316-317.
- 28 W. R. Zipfel, R. M. Williams, R. Christie, A. Y. Nikitin, B. T. Hyman and W. W. Webb, Proc. Natl. Acad. Sci. U. S. A., 2003, 100, 7075-7080.
- 29 S. A. Hilderbrand and R. Weissleder, Curr. Opin. Chem. Biol., 2010, 14, 71-79.
- 30 W. Denk, J. H. Strickler and W. W. Webb, Science, 1990, 248, 73-76.
- 31 H. M. Kim and B. R. Cho, Chem. Rev., 2015, 115, 5014-5055.
- 32 M. Pawlicki, H. A. Collins, R. G. Denning and H. L. Anderson, Angew. Chem., Int. Ed., 2009, 48, 3244-3266.
- 33 W. R. Zipfel, R. M. Williams and W. W. Webb, Nat. Biotechnol., 2003, 21, 1369-1377.
- 34 H. M. Kim and B. R. Cho, Chem. Commun., 2009, 153-164.
- 35 G. H. Patterson and D. W. Piston, Biophys. J., 2000, 78, 2159-2162.
- 36 H. Lai, M. Luo, Y. Xu, J. Pieprzyk, L. Pan, J. Zhang and M. A. Orgun, Laser Phys., 2019, 29, 055201.
- 37 L. Yuan, W. Lin, K. Zheng and S. Zhu, Acc. Chem. Res., 2013, 46, 1462-1473.
- 38 X. Wu, Z. Li, L. Yang, J. Han and S. Han, Chem. Sci., 2013, 4, 460-467.
- 39 X. Jia, Q. Chen, Y. Yang, Y. Tang, R. Wang, Y. Xu, W. Zhu and X. Qian, J. Am. Chem. Soc., 2016, 138, 10778-10781.
- 40 D. Cheng, Y. Pan, L. Wang, Z. Zeng, L. Yuan, X. Zhang and Y.-T. Chang, J. Am. Chem. Soc., 2017, 139, 285–292.
- 41 A. T. Aron, M. O. Loehr, J. Bogena and C. J. Chang, J. Am. Chem. Soc., 2016, 138, 14338-14346.
- 42 J. M. Fukuto, S. J. Carrington, D. J. Tantillo, J. G. Harrison, L. J. Ignarro, B. A. Freeman, A. Chen and D. A. Wink, Chem. Res. Toxicol., 2012, 25, 769-793.
- 43 R. Wang, Physiol. Rev., 2012, 92, 791-896.
- 44 P. Ou, R. Zhang, Z. Liu, X. Tian, G. Han, B. Liu, Z. Hu and Z. Zhang, Angew. Chem., Int. Ed., 2019, 58, 2261-2265.
- 45 Y. Luo, B. Bolon, S. Kahn, B. D. Bennett, S. Babu-Khan, P. Denis, W. Fan, H. Kha, J. Zhang, Y. Gong, L. Martin,

Perspective

- J.-C. Louis, Q. Yan, W. G. Richards, M. Citron and R. Vassar, *Nat. Neurosci.*, 2001, 4, 231–232.
- 46 S. Lesné, M. T. Koh, L. Kotilinek, R. Kayed, C. G. Glabe, A. Yang, M. Gallagher and K. H. Ashe, *Nature*, 2006, 440, 352–357
- 47 L. Ge, Z. Liu and Y. Tian, Chem. Sci., 2020, 11, 2215-2224.
- 48 V. Marx, Nat. Methods, 2017, 14, 949-953.
- 49 J. F. Callan, A. P. de Silva and D. C. Magri, *Tetrahedron*, 2005, **61**, 8551–8588.
- 50 M. H. Lee, J. S. Kim and J. L. Sessler, *Chem. Soc. Rev.*, 2015, 44, 4185–4191.
- 51 H. S. Jung, P. Verwilst, W. Y. Kim and J. S. Kim, *Chem. Soc. Rev.*, 2016, 45, 1242–1256.
- 52 X. Wu, L. Li, W. Shi, Q. Gong and H. Ma, *Angew. Chem., Int. Ed.*, 2016, 55, 14728–14732.
- 53 K. Gu, Y. Xu, H. Li, Z. Guo, S. Zhu, S. Zhu, P. Shi, T. D. James, H. Tian and W.-H. Zhu, *J. Am. Chem. Soc.*, 2016, 138, 5334–5340.
- 54 Z.-R. Dai, G.-B. Ge, L. Feng, J. Ning, L.-H. Hu, Q. Jin, D.-D. Wang, X. Lv, T.-Y. Dou, J.-N. Cui and L. Yang, *J. Am. Chem. Soc.*, 2015, 137, 14488–14495.
- 55 J. Ning, W. Wang, G. Ge, P. Chu, F. Long, Y. Yang, Y. Peng, L. Feng, X. Ma and T. D. James, *Angew. Chem.*, *Int. Ed.*, 2019, 58, 9959–9963.
- 56 J. Ning, T. Liu, P. Dong, W. Wang, G. Ge, B. Wang, Z. Yu, L. Shi, X. Tian, X. Huo, L. Feng, C. Wang, C. Sun, J. Cui, T. D. James and X. Ma, J. Am. Chem. Soc., 2019, 141, 1126–1134.
- 57 J. Ning, T. Liu, P. Dong, W. Wang, G. Ge, B. Wang, Z. Yu, L. Shi, X. Tian, X. Huo, L. Feng, C. Wang, C. Sun, J. Cui, T. D. James and X. Ma, *J. Am. Chem. Soc.*, 2019, **141**, 13278.
- 58 X. Jiao, Y. Li, J. Niu, X. Xie, X. Wang and B. Tang, *Anal. Chem.*, 2018, **90**, 533–555.
- 59 L. Wu, A. C. Sedgwick, X. Sun, S. D. Bull, X.-P. He and T. D. James, Acc. Chem. Res., 2019, 52, 2582–2597.
- 60 X. Wang, P. Li, Q. Ding, C. Wu, W. Zhang and B. Tang, Angew. Chem., Int. Ed., 2019, 58, 4674–4678.
- 61 L. C. Murfin, M. Weber, S. J. Park, W. T. Kim, C. M. Lopez-Alled, C. L. McMullin, F. Pradaux-Caggiano, C. L. Lyall, G. Kociok-Köhn, J. Wenk, S. D. Bull, J. Yoon, H. M. Kim, T. D. James and S. E. Lewis, *J. Am. Chem. Soc.*, 2019, 141, 19389–19396.
- 62 A. Sikora, J. Zielonka, M. Lopez, J. Joseph and B. Kalyanaraman, *Free Radical Biol. Med.*, 2009, 47, 1401–1407.
- 63 H. Chen, Y. Tang, M. Ren and W. Lin, *Chem. Sci.*, 2016, 7, 1896–1903.
- 64 L. Long, M. Huang, N. Wang, Y. Wu, K. Wang, A. Gong, Z. Zhang and J. L. Sessler, *J. Am. Chem. Soc.*, 2018, **140**, 1870–1875.
- 65 G. Fukuhara, J. Photochem. Photobiol., C, 2020, 42, 100340.
- 66 L. Yuan, F. Jin, Z. Zeng, C. Liu, S. Luo and J. Wu, *Chem. Sci.*, 2015, **6**, 2360–2365.
- 67 H. Shizuka, M. Nakamura and T. Morita, *J. Phys. Chem.*, 1979, **83**, 2019–2024.
- 68 Y.-C. Wang and H. Morawetz, *J. Am. Chem. Soc.*, 1976, **98**, 3611–3615.

- 69 W. Zhang, Z. Ma, L. Du and M. Li, *Analyst*, 2014, **139**, 2641–2649.
- 70 W. Sun, M. Li, J. Fan and X. Peng, Acc. Chem. Res., 2019, 52, 2818–2831.
- 71 M. Yang, J. Fan, J. Zhang, J. Du and X. Peng, *Chem. Sci.*, 2018, 9, 6758–6764.
- 72 C. G. Schalkwijk and C. D. A. Stehouwer, *Physiol. Rev.*, 2020, 100, 407–461.
- 73 S. H. Snyder, Science, 1992, 257, 494-496.
- 74 S. Jasid, M. Simontacchi, C. G. Bartoli and S. Puntarulo, *Plant Physiol.*, 2006, **142**, 1246–1255.
- 75 J. Miao, Y. Huo, X. Lv, Z. Li, H. Cao, H. Shi, Y. Shi and W. Guo, *Biomaterials*, 2016, **78**, 11–19.
- 76 Y. Huo, J. Miao, J. Fang, H. Shi, J. Wang and W. Guo, *Chem. Sci.*, 2019, **10**, 145–152.
- 77 S. G. Rhee, Science, 2006, 312, 1882-1883.
- 78 S. I. Reja, M. Gupta, N. Gupta, V. Bhalla, P. Ohri, G. Kaur and M. Kumar, *Chem. Commun.*, 2017, **53**, 3701–3704.
- 79 Y. Jiao, J. Yin, H. He, X. Peng, Q. Gao and C. Duan, *J. Am. Chem. Soc.*, 2018, **140**, 5882–5885.
- 80 P. Liu, J. Xu, D. Yan, P. Zhang, F. Zeng, B. Li and S. Wu, *Chem. Commun.*, 2015, 51, 9567–9570.
- 81 W. Sun, M. Li, J. Fan and X. Peng, Acc. Chem. Res., 2019, 52, 2818–2831.
- 82 A. Weller, Naturwissenschaften, 1955, 42, 175-176.
- 83 V. S. Padalkar and S. Seki, *Chem. Soc. Rev.*, 2016, 45, 169–202.
- 84 J. E. Kwon and S. Y. Park, Adv. Mater., 2011, 23, 3615–3642.
- 85 B. Dick and N. P. Ernsting, *J. Phys. Chem.*, 1987, **91**, 4261–4265.
- 86 T. Iijima, A. Momotake, Y. Shinohara, T. Sato, Y. Nishimura and T. Arai, *J. Phys. Chem. A*, 2010, **114**, 1603–1609.
- 87 X. Li, R.-R. Tao, L.-J. Hong, J. Cheng, Q. Jiang, Y.-M. Lu, M.-H. Liao, W.-F. Ye, N.-N. Lu, F. Han, Y.-Z. Hu and Y.-H. Hu, J. Am. Chem. Soc., 2015, 137, 12296–12303.
- 88 L. Wu, Y. Wang, M. Weber, L. Liu, A. C. Sedgwick, S. D. Bull, C. Huang and T. D. James, *Chem. Commun.*, 2018, 54, 9953– 9956.
- 89 L. Wu, Q. Yang, L. Liu, A. C. Sedgwick, A. J. Cresswell, S. D. Bull, C. Huang and T. D. James, *Chem. Commun.*, 2018, 54, 8522–8525.
- 90 P. Zhang, C. Fu, Q. Zhang, S. Li and C. Ding, *Anal. Chem.*, 2019, **91**, 12377–12383.
- 91 W. Feng, S. Feng and G. Feng, *Anal. Chem.*, 2019, **91**, 8602–8606.
- 92 C. C. Romão, W. A. Blättler, J. D. Seixas and G. J. L. Bernardes, *Chem. Soc. Rev.*, 2012, **41**, 3571–3583.
- 93 A. C. Sedgwick, W.-T. Dou, J.-B. Jiao, L. Wu, G. T. Williams, A. T. A. Jenkins, S. D. Bull, J. L. Sessler, X.-P. He and T. D. James, *J. Am. Chem. Soc.*, 2018, 140, 14267–14271.
- 94 Y. Hong, J. W. Y. Lam and B. Z. Tang, *Chem. Commun.*, 2009, 4332–4353.
- 95 J. Luo, Z. Xie, J. W. Y. Lam, L. Cheng, H. Chen, C. Qiu, H. S. Kwok, X. Zhan, Y. Liu, D. Zhu and B. Z. Tang, *Chem. Commun.*, 2001, 1740–1741.
- 96 J. Mei, Y. Hong, J. W. Y. Lam, A. Qin, Y. Tang and B. Z. Tang, Adv. Mater., 2014, 26, 5429–5479.

97 Y. Hong, J. W. Y. Lam and B. Z. Tang, *Chem. Soc. Rev.*, 2011, 40, 5361–5388.

Chemical Science

- 98 C. Zhu, R. T. K. Kwok, J. W. Y. Lam and B. Z. Tang, *ACS Appl. Bio Mater.*, 2018, **1**, 1768–1786.
- 99 J. Wang, C. Li, Q. Chen, H. Li, L. Zhou, X. Jiang, M. Shi, P. Zhang, G. Jiang and B. Z. Tang, *Anal. Chem.*, 2019, 91, 9388–9392.
- 100 W. Qin, N. Alifu, Y. Cai, J. W. Y. Lam, X. He, H. Su, P. Zhang, J. Qian and B. Z. Tang, *Chem. Commun.*, 2019, 55, 5615– 5618
- 101 J. Liu, C. Chen, S. Ji, Q. Liu, D. Ding, D. Zhao and B. Liu, Chem. Sci., 2017, 8, 2782–2789.
- 102 A. Shao, Y. Xie, S. Zhu, Z. Guo, S. Zhu, J. Guo, P. Shi, T. D. James, H. Tian and W.-H. Zhu, *Angew. Chem., Int. Ed.*, 2015, 54, 7275–7280.
- 103 J. Ouyang, L. Sun, Z. Zeng, C. Zeng, F. Zeng and S. Wu, *Angew. Chem., Int. Ed.*, 2020, **59**, 10111–10121.
- 104 W. Fu, C. Yan, Z. Guo, J. Zhang, H. Zhang, H. Tian and W.-H. Zhu, J. Am. Chem. Soc., 2019, 141, 3171–3177.
- 105 X. Jiang, L. Wang, S. L. Carroll, J. Chen, M. C. Wang and J. Wang, *Antioxid. Redox Signaling*, 2018, **29**, 518–540.
- 106 Z. Guo, S. Park, J. Yoon and I. Shin, *Chem. Soc. Rev.*, 2014, 43, 16–29.

- 107 J. Wu, W. Liu, J. Ge, H. Zhang and P. Wang, *Chem. Soc. Rev.*, 2011, **40**, 3483–3495.
- 108 T. V. Mishanina, M. Libiad and R. Banerjee, *Nat. Chem. Biol.*, 2015, **11**, 457-464.
- 109 W. Chen, A. Pacheco, Y. Takano, J. J. Day, K. Hanaoka and M. Xian, *Angew. Chem.*, *Int. Ed.*, 2016, 55, 9993–9996.
- 110 W. Zhang, F. Huo, F. Cheng and C. Yin, *J. Am. Chem. Soc.*, 2020, **142**, 6324–6331.
- 111 K. Dhara, S. Lohar, A. Patra, P. Roy, S. K. Saha, G. C. Sadhukhan and P. Chattopadhyay, *Anal. Chem.*, 2018, **90**, 2933–2938.
- 112 Q. Hu, M. Gao, G. Feng and B. Liu, *Angew. Chem., Int. Ed.*, 2014, 53, 14225–14229.
- 113 B. C. Dickinson and C. J. Chang, *J. Am. Chem. Soc.*, 2008, 130, 9638–9639.
- 114 W. Fu, C. Yan, Y. Zhang, Y. Ma, Z. Guo and W.-H. Zhu, *Front. Chem.*, 2019, 7, 291.
- 115 X. Shi, N. Yan, G. Niu, S. H. P. Sung, Z. Liu, J. Liu, R. T. K. Kwok, J. W. Y. Lam, W.-X. Wang, H. H.-Y. Sung, I. D. Williams and B. Z. Tang, *Chem. Sci.*, 2020, 11, 3152–3163.